Geologica Acta, Vol.4, Nº1-2, 2006, 123-150
Available online at www.geologica-acta.com

geologica acta

Geology, age and tectonic evolution of the Sierra Maestra Mountains, southeastern Cuba

Y. ROJAS-AGRAMONTE [1,2] F. NEUBAUER [3] A.V. BOJAR [4] E. HEJL [3] R. HANDLER [3] and D.E. GARCÍA-DELGADO [5]

[1] **Institut für Geowissenschaften, Universität Mainz**
D-55099 Mainz, Germany. E-mail: rojas@uni-mainz.de

[2] **Tectonics Special Research Centre, University of Western Australia**
35 Stirling Highway, Crawley, WA 6009, Australia. E-mail: rojas@uni-mainz.de

[3] **Fachbereich Geographie, Geologie und Mineralogie, Universität Salzburg**
Hellbrunner Strasse 34, A-5020 Salzburg, Austria. Neubauer E-mail: franz.neubauer@sbg.ac.at
Hejl E-mail: ewald.hejl@sbg.ac.at Handler E-mail: robert.handler@sbg.ac.at

[4] **Institut für Geologie und Paläontologie, Universität Graz**
Heinrichstr. 26, A-8010 Graz, Austria. E-mail: ana-voica.bojar@uni-graz.at

[5] **Instituto de Geología y Paleontología**
Centro de Investigaciones del Petroleo (CEINPET), Washington 169, Cerro, Havana 12000, Cuba. E-mail: dora@ceinpet.cupet.cu

ABSTRACT

We summarize the available geological information on the Sierra Maestra Mountains in southeastern Cuba and report new zircon fission track and biotite Ar-Ar ages for this region. Two different and genetically unrelated volcanic arc sequences occur in the Sierra Maestra, one Cretaceous in age (pre-Maastrichtian) and restricted to a few outcrops on the southern coast, and the other Palaeogene in age, forming the main expression of the mountain range. These two sequences are overlain by middle to late Eocene siliciclastic, carbonatic and terrigenous rocks as well as by late Miocene to Quaternary deposits exposed on the southern flank of the mountain range. These rocks are britle deformed and contain extension gashes filled with calcite and karst material. The Palaeogene volcanic arc successions were intruded by calc-alkaline, low- to medium-K tonalites and trondhjemites during the final stages of subduction and subsequent collision of the Caribbean oceanic plate with the North American continental plate. U-Pb SHRIMP single zircon dating of five granitoid plutons yielded $^{206}Pb/^{238}U$ emplacement ages between 60.5 ± 2.2 and 48.3 ± 0.5 Ma. These granitoids were emplaced at pressures ranging from 1.8 to 3.0 kbar, corresponding to depths of ca. 4.5-8 km. $^{40}Ar/^{39}Ar$ dating of two biotite concentrates yielded ages of 50 ± 2 and 54 ± 4 Ma, indicating cooling through ca. 300 ºC. Zircon and apatite fission track ages range from 32 ± 3 to 46 ± 4 Ma and 31 ± 10 to 44 ± 13 Ma, respectively, and date cooling through 250 ± 50 ºC and 110 ± 20 ºC. The granitoids are the result of subduction-related magmatism and have geochemical characteristics similar to those of magmas from intra-oceanic island-arcs such as the Izu Bonin-Mariana arc and the New Britain island arc. Major and trace element patterns suggest evolution of these rocks from a single

magmatic source. Geochemical features characterize these rocks as typical subduction-related granitoids as found worldwide in intra-oceanic arcs, and they probably formed through fractional crystallization of mantle-derived low- to medium-K basalts. Several distinct phases of deformation were recognized in the Sierra Maestra, labelled D_1 to D_6, which define the transition from collision of the Palaeogene island arc to the formation of the Oriente Transform Wrench Corridor south of Cuba and later movement of the Caribbean plate against the North American plate. The first phase (D_1) is related to the intrusion of a set of extensive subparallel, N-trending subvertical basalt-andesite dykes, probably during the early to middle Eocene. Between the late-middle Eocene and early Oligocene (D_2), rocks of the Sierra Maestra were deformed by approximately east-west trending folds and north-vergent thrust faults. This deformation (D_2) was linked to a shift in the stress regime of the Caribbean plate from mainly NNE-SSW to E-W. This shift in plate motion caused the abandonment of the Nipe-Guacanayabo fault system in the early Oligocene and initiation of a deformation front to the south where the Oriente Transform Wrench corridor is now located. Compressive structures were overprinted by widespread extensional structures (D_3), mainly faults with southward-directed normal displacement in the Oligocene to early Miocene. During this period the plate boundary jumped to the Oriente fault. This event was followed by transpressive and transtensive structures (D_4–D_6) due to further development of the sinistral E-trending Oriente Transform wrench corridor. These structures are consistent with oblique convergence in a wide zone of left-lateral shear along an E-W-oriented transform fault.

KEYWORDS | **Cuba. Calc-alkaline granitoids. Geochronology. Palaeostress analysis. Subduction magmatism. Transform fault. Wrench corridor.**

INTRODUCTION

The geological framework and tectonic evolution of Cuba, the only island in the Greater Antilles located on the North American plate (Fig. 1A), appears to be the most complex within the northern Caribbean realm. The geology of Cuba differs from that of other islands in the Caribbean in that rare Precambrian rocks occur in the north-central part of the island which have not been reported from other Caribbean regions (Somin and Millán, 1977; Renne et al., 1989; Draper and Barros, 1994; Iturralde-Vinent, 1994). Although continental margin sedimentary rocks of Jurassic to Cretaceous age and different types of Mesozoic metamorphic and volcano-plutonic complexes also occur on other Caribbean islands, they are particularly widespread in Cuba (Iturralde-Vinent, 1996a).

Cuba largely comprises from NNE to SSW (1) Jurassic to late Cretaceous carbonates, evaporites and cherts from the Bahamas Platform, (2) the late Triassic?–early Cretaceous Northern Ophiolite belt, (3) the Cretaceous Volcanic Arc, (4) Mesozoic metamorphic complexes or terranes, and (5) a Palaeogene Volcanic Arc (Iturralde-Vinent, 1996a, b), constituting together the Cuban Orogen. This orogen was accreted to the North American continental margin during late Cretaceous to Eocene tectonic process (Iturralde-Vinent, 1994, 1998).

The eastern part of Cuba, east of the Nipe-Guacanayabo fault zone (Fig. 1B), represents a key element of the northern Caribbean domain with distinct characteristics different from other areas of the island. According to Iturralde-Vinent (2003) this area is the only domain in Cuba where rocks of the Bahamas platform (North American plate) are metamorphosed (Fig. 1B) and where Cretaceous Volcanic Arc rocks were partially metamorphosed under HP/LT conditions. In particular, it is the only area of Cuba where ophiolitic rocks are almost horizontally disposed. A well developed Palaeogene Volcanic Arc (PVA), with the axial zone well exposed in the Sierra Maestra Mountains, is a further unique characteristic of eastern Cuba (Fig. 1B). Palaeogene volcano-sedimentary sequences to the north of the Sierra Maestra have been interpreted as the back arc zone of the PVA (Iturralde-Vinent, 1994, 1998, Fig. 1B). Due to these reasons, this region is known as the Eastern Cuban Microplate (ECM; Iturralde-Vinent, 2003). The rocks of the ECM were considerably deformed during the latest Cretaceous (Iturralde-Vinent, 2003), in the latest Eocene to Oligocene and again during the Miocene (Rojas-Agramonte et al., 2005).

The Sierra Maestra is composed of minor Cretaceous arc-related rocks unconformably overlain by widespread Palaeogene volcanic arc successions which, in turn, are followed by middle to late Eocene clastic and carbonate rocks (Figs. 2A and 3). The southern part of the Sierra Maestra exposes several granitoid massifs which were intruded into the PVA during the waning phases of arc magmatism (Rojas-Agramonte et al., 2004; see Fig. 2A). The PVA also extends to other Caribbean islands such as Hispaniola, Jamaica, Puerto Rico, the Lesser Antilles, Nicaraguan Rise and Aves Ridge (Fig. 1A; Jackson and Smith, 1979; Case

et al., 1984; Dengo and Case, 1990; Iturralde-Vinent, 1996a, b), but the most extensive outcrops of Palaeogene volcanic rocks appear in eastern Cuba.

The Sierra Maestra is an E-W trending mountain range (Fig. 2A) that occurs immediately north of the North Caribbean (Oriente) transform system (Hernández-Santana et al., 1991; Figs. 1A and 2A), extending from several km west of Pilón to the Guantánamo basin (Fig. 1B) and stretching ca. 190 km E–W and ca. 20 km N–S. This transform system separates the Caribbean plate from the North American plate and it is connected with the

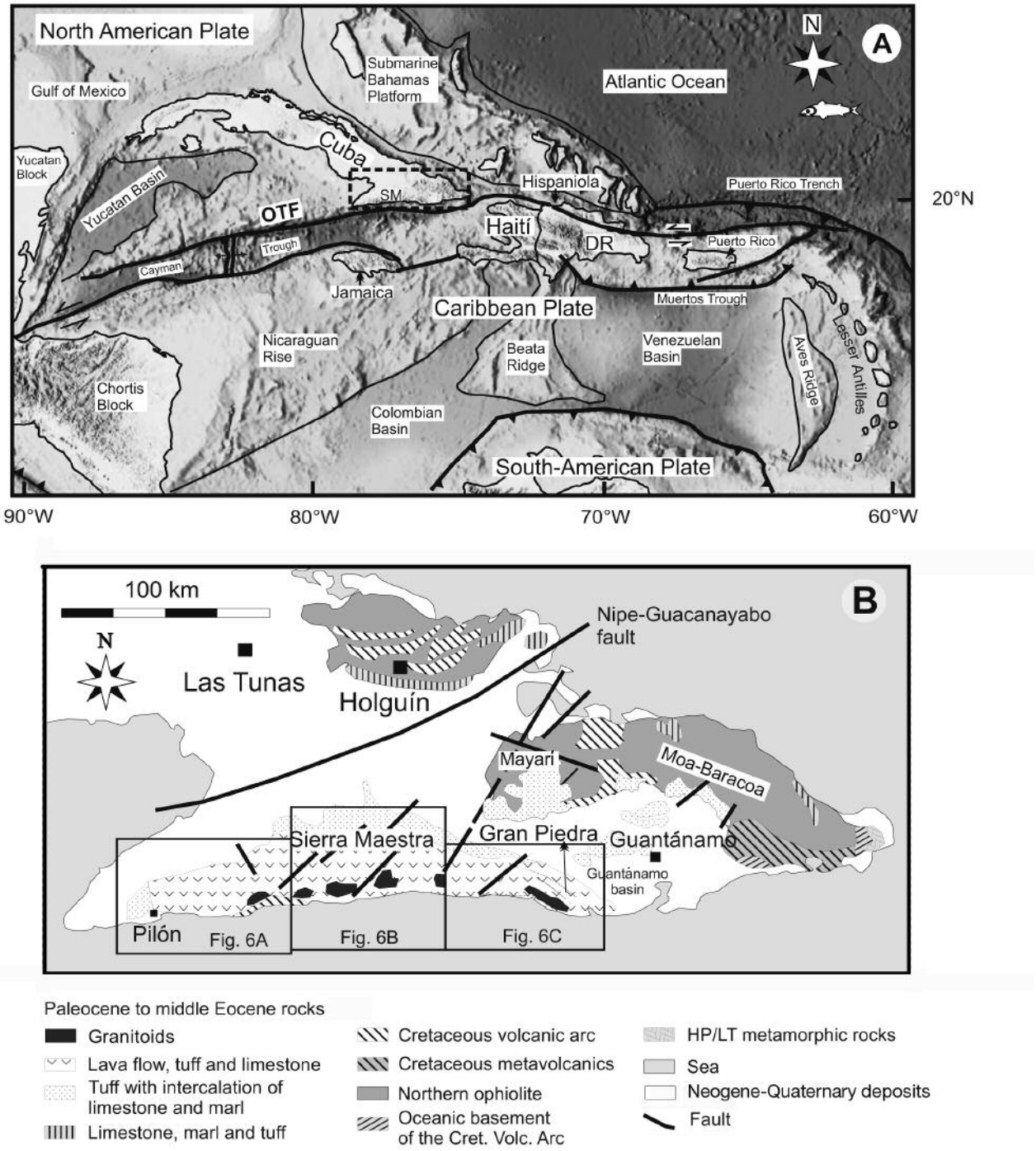

FIGURE 1 | **A) Bathymetric map of the Caribbean showing main features of the region and location of the Oriente Fault (after USGS Coastal & Marine Geology Program: CMG InfoBank Atlas: Caribbean Sea region). Dashed rectangle locates eastern province of Cuba, which is shown in detail in Figure 1B. Abbreviations: SM: Sierra Maestra; DR: Dominican Republic, OTF: Oriente Transform Fault. B) Geological sketch map of eastern Cuba (after Iturralde-Vinent, 1996a). The insets show figure numbers of detailed structural maps.**

Swan fault to the west through the Mid-Cayman spreading centre (Fig. 1A). Since the latest middle Eocene this spreading centre has generated the oceanic crust of the Cayman trough (Rosencrantz et al., 1988; Fig. 1A). A steep topographic gradient is typical for this region, as indicated by the highest elevation of ca. 1974 m (Pico Turquino) (Fig. 2A) and the lowest depression of –6642 m in the adjacent Oriente Deep to the S (Fig. 2A). This relief is due to Neogene sinistral strike-slip activity along the Oriente transform system which we named the Oriente Transform Wrench Corridor (OTWC, Rojas-Agramonte et al., 2005; Fig. 2A). The Neogene-Quaternary Santiago basin (Fig. 2A) divides the Sierra Maestra into two main tectonic blocks, one to the west and the Gran Piedra block to the east (Pérez-Pérez and García-Delgado, 1997). Sinistral movement along the OTWC was responsible for the present configuration of the Sierra Maestra macroblock (Hernández et al., 1989; Fig. 2B). NE-trending faults and subordinate ENE-WSW-trending faults formed in response to this movement and are important elements in the region, determining some geomorphologic and dynamic features in this area (Hernández-Santana et al., 1991; Rueda et al., 1994).

GEOLOGICAL SETTING OF THE SIERRA MAESTRA MOUNTAIN RANGE

The main part of the Sierra Maestra represents a Palaeogene island arc formed during early Palaeocene to

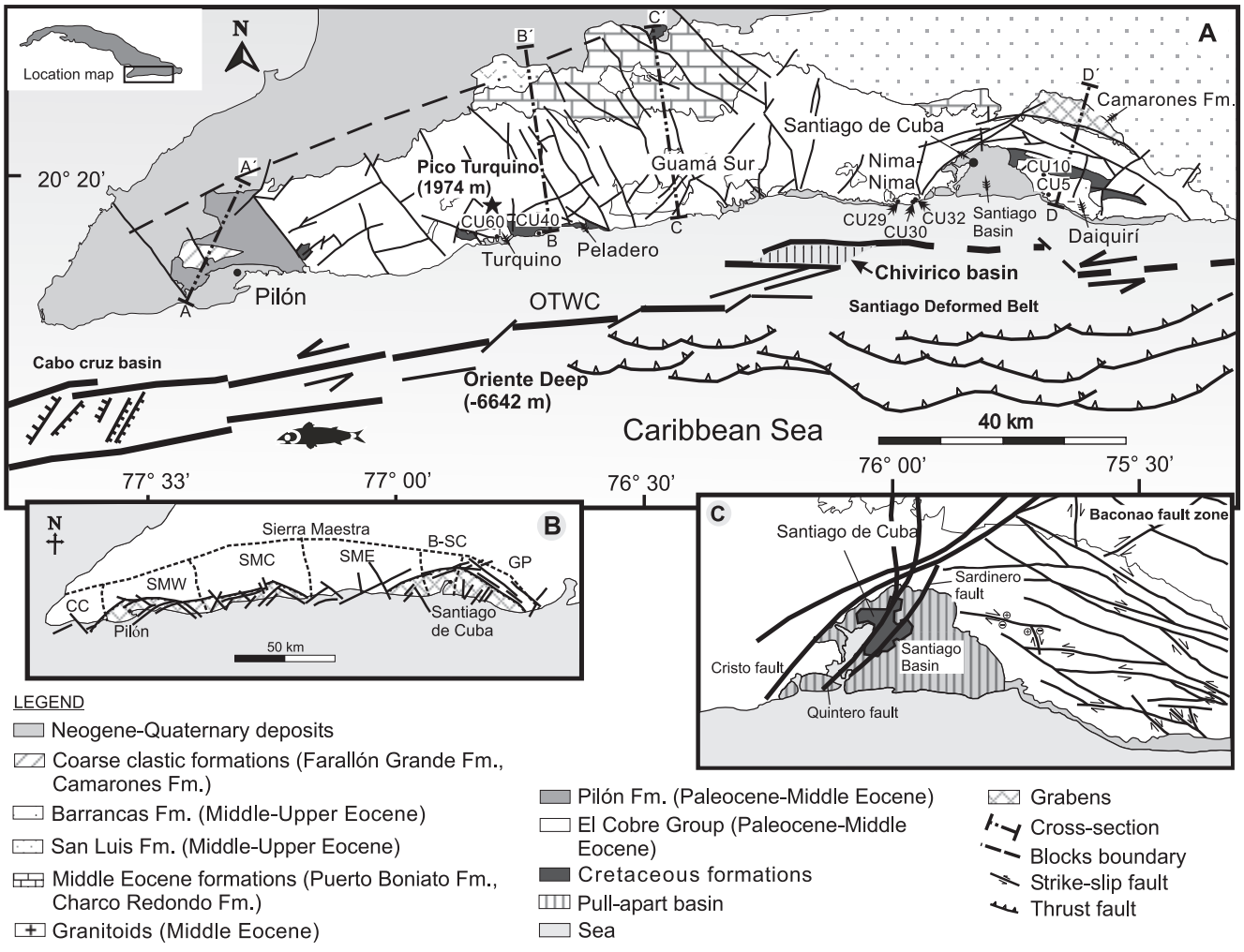

FIGURE 2 | **Simplified geological map of the Sierra Maestra (after Pérez-Pérez and García-Delgado, 1997) and the submarine sectors of the Cuban continental margin, showing distribution of main tectonic elements along the Oriente Transform Fault (after Calais et al., 1998). Location of cross-sections (A-A´–D-D´) is also shown. OTWC: Oriente Tranform Wrench Corridor. B) Morphotectonic differentiation in the Sierra Maestra macroblock: CC: Cabo Cruz; SMW: Western Sierra Maestra; SMC: Central Sierra Maestra; SME: Eastern Sierra Maestra; B-SC: Baconao-Santiago de Cuba, GP: Gran Piedra (after Hernández-Santana et al., 1991; Iturralde-Vinent, 1991; Rojas-Agramonte et al., 2005). C) Inset map showing main fault pattern in and around the Santiago basin (after Rueda-Pérez et al., 1994; Rojas-Agramonte et al., 2005). The most important fault system is that with NE-SW orientation followed by the Baconao fault zone system with a NW-SE orientation.**

middle Eocene times (Pérez-Pérez and García-Delgado, 1997). The arc was subsequently disrupted during the Neogene along strike of the Sierra Maestra through initiation of the OTWC. Palaeogene volcanic activity was limited to the eastern part of the island and is represented by a thicker than 4000 m volcanic rocks sequence (Cazañas et al., 1998). A large number of hypabyssal bodies of dioritic to granitic composition and plutons of gabbro, quartz-diorite, tonalite, granodiorite and granite intruded the Palaeogene volcanic sequence (Laznicka et al., 1970; Rodríguez-Crombet et al., 1997). The stratigraphy of the Palaeocene to late Eocene rocks in the Sierra Maestra is shown in Fig. 3 (see Cazañas et al., 1998 and Rojas-Agramonte et al., 2004 for further details). The southern mar-

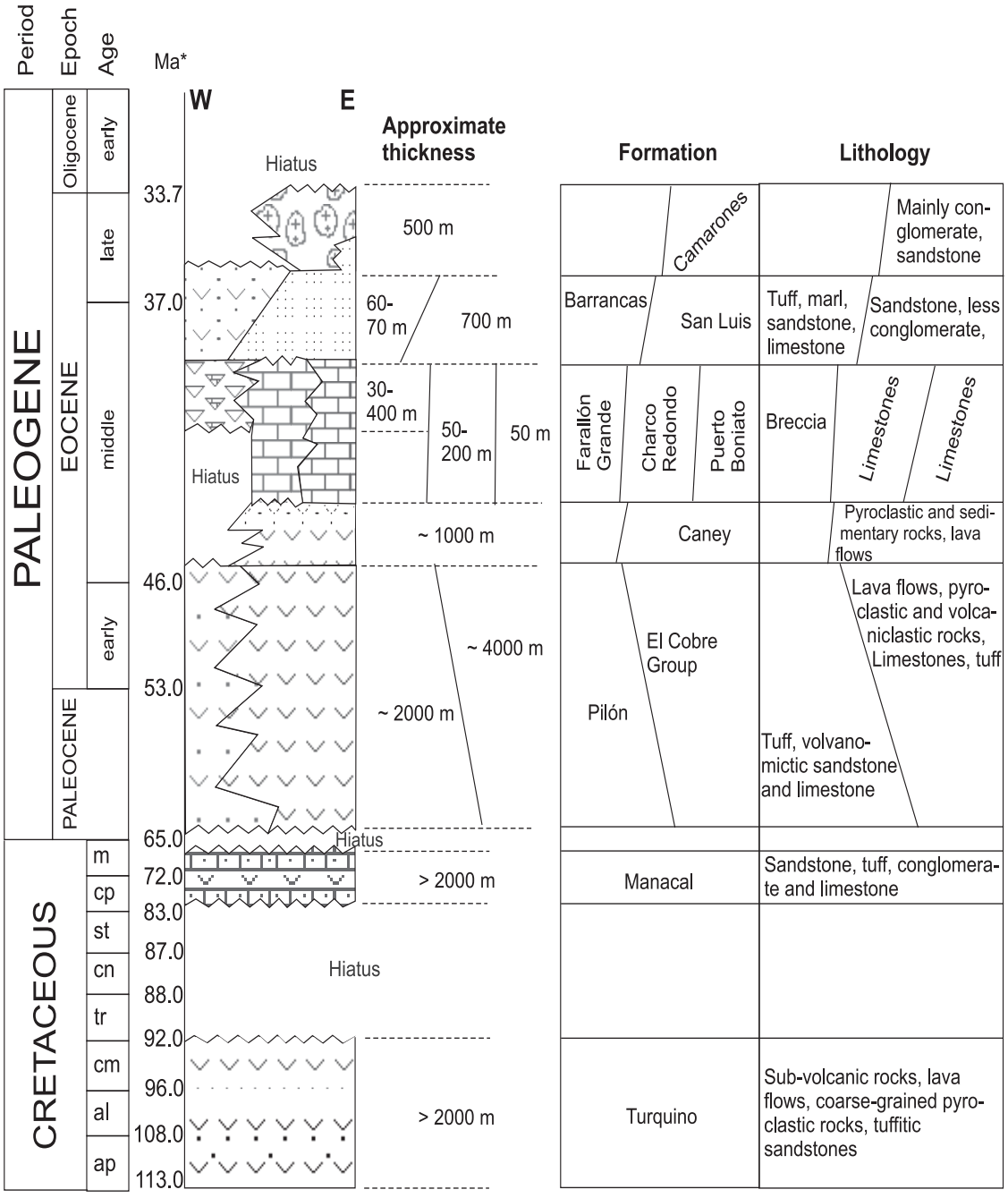

FIGURE 3 | **Stratigraphic column of Cretaceous to Palaeogene formations in the Sierra Maestra (after Rojas-Agramonte et al., 2004). *Geological time scale, calibration after Remane et al. (2002). Abbreviations: ap: Aptian; al: Albian; cm: Cenomanian; tr: Turonian; cn: Coniacian; st: Santonian; cp: Campanian; m: Maastrichtian.**

gin of the Sierra Maestra also exposes late Miocene to Quaternary rocks, filling several depressions (grabens) facing the OTWC (Fig. 2B). These young formations unconformably overlay Cretaceous to Eocene rocks (Fig. 2A). The late Miocene to Quaternary formations appear to be less deformed than the pre-Neogene rocks. The stratigraphy of the late Miocene to Quaternary rocks is shown in Fig. 4 and has been described in detail by Cabrera Castellanos et al. (2003) and Rojas-Agramonte et al. (2005). Neotectonic movements related to the OTWC and eustatic sea level changes controlled sedimentation of the Upper Miocene–Quaternary formations.

The rocks in the Sierra Maestra are deformed with increasing intensity from south to north (Fig. 5). Oligocene rocks to the north of the mountain range show only mild deformation (Iturralde-Vinent, 1996b). The dominant structure is a large N-dipping monocline, complicated in the eastern and western parts by synforms and antiforms (Fig. 5). Major granitoid massifs are exposed in its southern part and more open folds in the north. Rojas-Agramonte et al. (submitted) found the following predominant fault orientations in the Sierra Maestra (Fig. 6): (1) Approximately NW-striking faults occur over the entire Sierra Maestra and display mainly dextral strike-slip displacement. Some of these faults are cut by NNW-oriented strike-slip faults. NW-striking faults with sinistral displacement were identified at some localities. All these faults postdate deposition of Middle to Upper Eocene formations. (2) NE-oriented dextral strike-slip faults also affect middle to Upper Eocene formations. (3) Approximately E-striking faults are dominant near the coast in the area of Pilón–Turquino (Fig. 6A). Because of cross-cutting relationships, these faults seem to postdate formation of folds which are dominant in that region. E-trending faults define two generations and types of slip: normal, S-directed motion (likely older) and sinistral displacement (likely younger) and (4) Approximately WSW-striking faults are predominant close the coast from east of La Mula to west of Santiago de Cuba (Fig. 6B). Some of these are thrust faults; some others are sinistral strike-slip faults, which overprint thrust faults at a few localities.

Reverse and thrust faults dominate the most northern section in the Gran Piedra block (Fig. 7A) whereas normal faults overprinting earlier structures prevail in the region close to the coast (Rojas-Agramonte et al., submitted; Fig. 7B). Individual faults are locally associated with alteration zones, which are several centimetres to several metres wide.

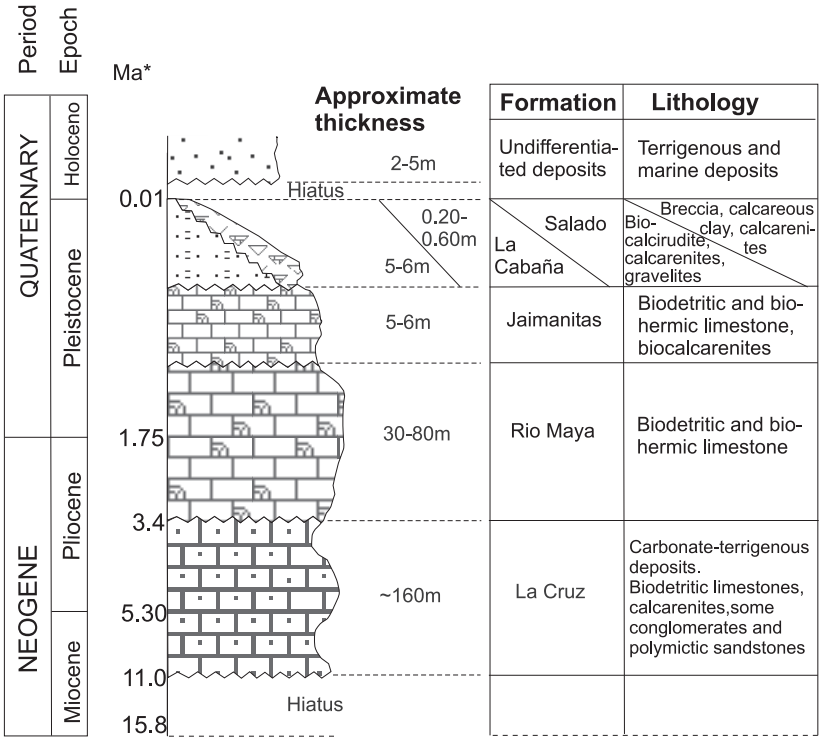

FIGURE 4 | **Stratigraphic column of late Miocene to Quaternary formations of the southern Sierra Maestra (after Rojas-Agramonte et al., 2005). *Geological time scale, calibration after Remane et al. (2002).**

Outcrop-scale folds are not frequent in the southern Sierra Maestra and appear to be associated with reverse faulting (Rojas-Agramonte et al., submitted). To the North of the Gran Piedra block an overturned fold trending E–W is developed in the San Luis Formation and is related to overthrusting and reverse faulting (Fig. 7C).

Many folds occur within well-stratified ash tuffs of the Pilón Formation (Fig. 7D), mainly isoclinal and open folds. These formed as a result of NE–SW contraction and have fold amplitudes as large as 10 metres (Rojas-Agramonte et al., submitted). Synsedimentary slump folds (with folded bedding dipping to the west) also occur in the Pilón Formation. These are layer-parallel, tight to isoclinal folds with fold axes trending ca. E–W; they are overturned and document transport from S to N. In the Gran Piedra block the fold structures have a constant NW-trend.

Geomorphology and neotectonics

The neotectonic fault system is mainly responsible for the present coastal configuration and for the formation of different morphostructural blocks in the Sierra Maestra (Fig. 2B). These blocks display strong fracturing in the way of horsts (Hernández-Santana et al., 1991) and grabens located in the southern sectors close to the coast (Iturralde-Vinent, 1991). The Central Sierra Maestra macroblock (SMC; Fig. 2B) is the most elevated in southeastern Cuba with the most intense neotectonic movements, whereas the Boniato-Santiago de Cuba block (B-SC; Fig. 2B) constitutes the link between the western Sierra Maestra and the Gran Piedra Mountains. The Santiago basin occurs in this block and is the most depressed graben in the region.

The Upper Miocene to Quaternary deposits generally increases in elevation, including several terraces (Rojas-

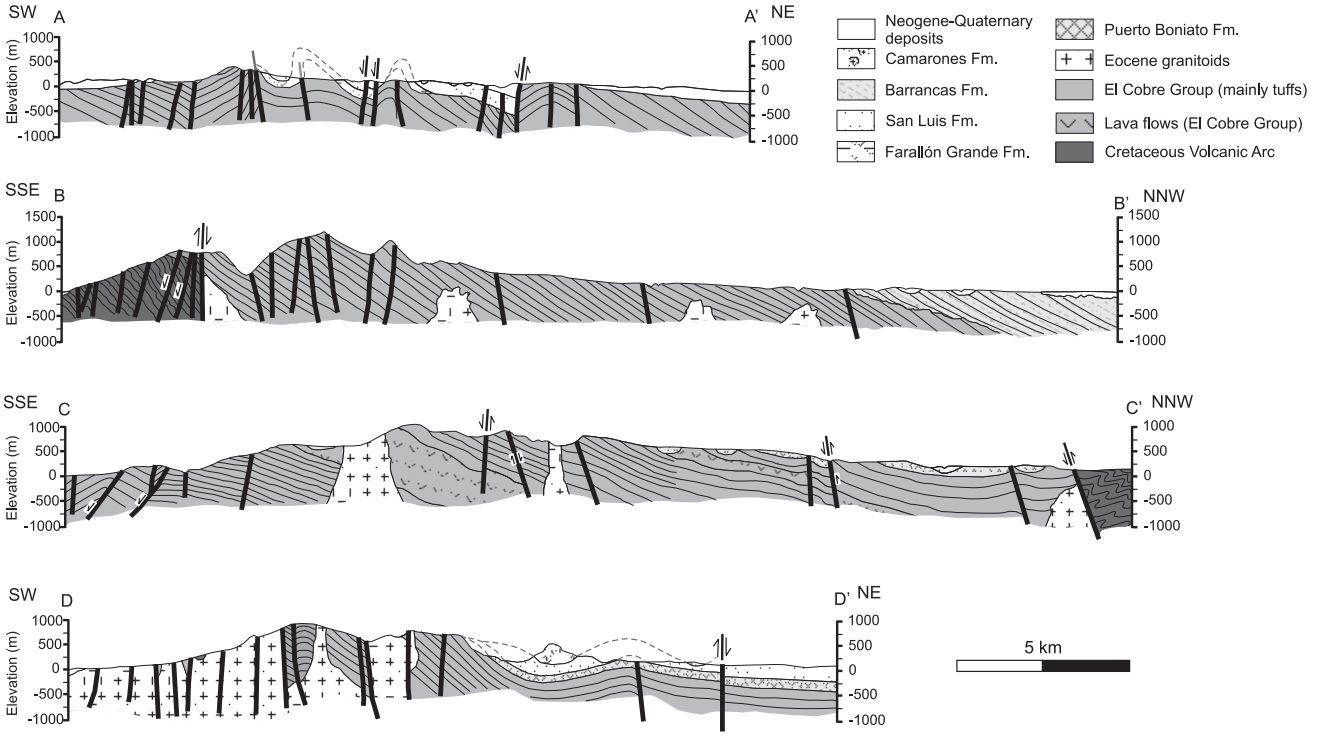

FIGURE 5 | **Cross-sections across the Sierra Maestra (after Rojas-Agramonte et al., submitted). See Figure 2 for location. In general, the Pilón area (cross-section A–A´) has a synclinal structure with the Farallón Grande and San Luis Formations cropping out in its centre and the Pilón Formation dominating this region (see Fig. 2A). Lava flows in this zone are scarce or practically absent, but small dykes and subvolcanic bodies of mafic composition occur within predominantly well-bedded ash tuffs. Cross-sections B–B´ and C–C´ show the main structures in the central part of the Sierra Maestra. The area exhibits a monoclinal structure with rocks generally dipping to the north. Some local changes in dip direction close to the coast are mainly related to normal faults and overturned folds. E–W trending folds are connected with reverse faults. Extensive outcrops of CVA rocks are typical in this area (cross-section B–B´) where granitoid bodies intrude the PVA and CVA successions or are in tectonic contact with these sequences. Cross–section D-D´ shows the Gran Piedra block where small relicts of the CVA are in contact with granitoid bodies of the PVA which are extensively exposed in this area. The Cretaceous volcanic rocks are difficult to recognize in the Gran Piedra block and also in the rest of the Sierra Maestra due to similarities with the PVA sequences. The rocks of the El Cobre Group in Gran Piedra dip northeast, and those from the Middle to Upper Eocene formations to the north. This is the most deformed part of the mountain range, due to possible clockwise rotation of the Gran Piedra block in the Neogene when the Santiago basin formed (Rojas-Agramonte et al., 2005). Large open folds appear to the north at a regional scale, folding the PVA and all Eocene formations.**

Agramonte et al., 2005). Terraces in the Jaimanitas Formation can be seen at several localities along the southeastern Cuban coast. In the Río Maya Formation up to four Plio-Pleistocene terrace levels have been identified. The terraces reach altitudes of up to 200 m in the eastern part of the area (Figs. 7E and E'). The deposits are faulted and fractured and contain subvertical calcite- and karst-filled tension gashes. Strike-slip and subordinate normal faults can be

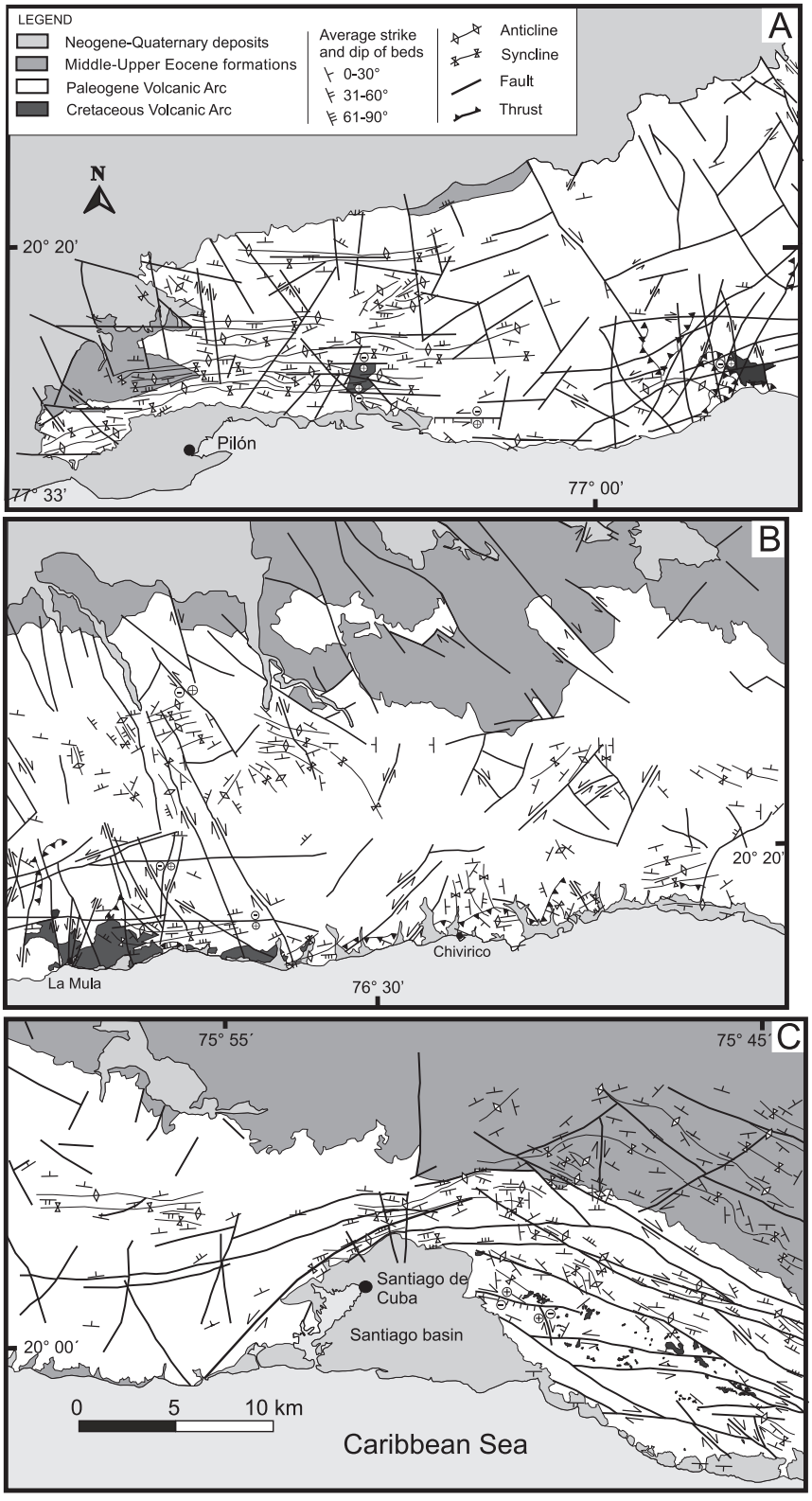

FIGURE 6 **A) Structural map showing main structures and fault pattern in the area of Pilón and part of the central Sierra Maestra (see Figure 1B for location; after Rojas-Agramonte et al., submitted). Three main fault systems appear dominant in this region, namely E-, NE- and NW- striking faults. In general terms, NW-trending faults are mainly dextral strike-slip, whereas E-striking faults are associated with normal faults with a dextral or sinistral component. Another conspicuous feature in this region is the formation of large-scale anticlines and synclines oriented E-W and formed during different phases of compressive deformation. Anticlines are generally tight with limbs varying in dip angles from 60° to 90°, whereas limbs in synclines dip at maximum angles of 40° to 50°. These folds are generally complicated by small-scale secondary folds having smooth limb inclinations. To the east of the area, and already part of central Sierra Maestra, there appear several N-trending thrust faults dipping to the west, whereas close to the coast the pattern changes to E-W trending thrusts dipping to the south. B) Structural sketch map of the central Sierra Maestra (see Figure 1B for location; after Rojas-Agramonte et al., submitted) showing main tectonic features of the area. The dominant structures are NW- and a major E-striking fault systems; subordinate are NE-striking sinistral faults. In comparison with the Pilón area, this region appears less complicated by small-scale synforms and antiforms and generally smooth dips of beds to the north (ca. 20° to 30°); fold axes mainly trend N, NE and E. A relevant feature close to the coast is the occurrence of south-dipping thrust faults parallel to the coast (cross-section C-C´, Fig. 5); N–S trending thrust faults appear to the west of this area. The distribution of faults is irregular near the coast, with different orientations; normal faults are common and reverse faults are subordinate. To the north a more consistent fault pattern with a NW-trending fault set has a dextral or sinistral component. C) Structural map of the region of Gran Piedra, eastern Sierra Maestra (see Figure 1B for location; after Rojas-Agramonte et al., submitted), showing the main fault and fold pattern. In general, the area east of Santiago de Cuba is characterized by a large-scale anticline-syncline, complicated by small secondary structures in the centre. The orientation of faults varies from NW, E and NE. NW-striking faults are the most common, and large-scale faults are up to 30 km long. NE-trending faults are common north of Gran Piedra and mainly affect Middle to Upper Eocene formations. Normal faults are common and locally are reactivated as dextral or sinistral strike-slip faults. The general dip direction of the rocks is to the north with angles varying from 0° to 40° in rocks of El Cobre Group and from 10° to 30° in the Middle to Upper Eocene formations. To the south and close to the coast, Neogene to Quaternary sedimentary rocks dip to the south at angles of 15° to 30°. To the west of Santiago de Cuba the pattern is different with a predominance of ENE- and NNW- to NNE-striking faults. Synclines and anticlines trend east.**

observed with offsets in the order of 0.1 to several metres (Rojas-Agramonte et al., 2005; Figs. 7F and 7G).

The still-active sinistral transcurrent El Cristo fault (Pérez-Pérez and García-Delgado, 1997; Fig. 2C) branches off to the NW from the late Miocene to Quaternary rocks in the Santiago basin. This fault is part of the OTWC and is defined as a synthetic Riedel fault (Pérez-Pérez and García-Delgado, 1997). The subsidence and depositional history of the Santiago basin was controlled by strike-slip deformation related to Miocene activity along the El Cristo fault as well as synsedimentary tectonics (Pérez-Pérez and García-Delgado, 1997). Late Miocene to Quaternary rocks are exposed in the Santiago basin (minimum thickness ca. 200 m).

GEOCHEMISTRY

Geochemistry of the El Cobre Group in the Sierra Maestra

The rocks of the El Cobre Group have been subdivided into three different sequences on account of their volcanogenic and geochemical features (Méndez-Calderón et al., 1994; Méndez-Calderón, 1997). According to Méndez-Calderón (1997), the lower sequence is characterized by intense explosive volcanism and lava flows. The dominant composition is basaltic and basaltic-andesitic with a tholeiitic trend. The middle sequence is dominated by rocks related to explosive volcanism with varying composition from andesitic to andesitic-basaltic, dacitic to rhyodacitic. This sequence is characterized by a tholeiitic to calc-alkaline trend. The upper sequence is characterized by explosive volcanism with lava flows with basaltic, andesitic-basaltic and dacitic-rhyodacitic composition and with a tholeiitic to calc-alkaline trend.

Cazañas et al. (1998) studied the lower and middle sequence of the El Cobre Group and found these volcanic rocks to be similar to low-K tholeiites of island arcs (IAT; see figs. 7A and 7B in Cazañas et al., 1998). The rocks analysed by Cazañas et al. (1998), following the classification of total alkalis versus silica, were basalt, basaltic andesite, andesite and dacite. The REE-content in these rocks is extremely low. A chondrite-normalized REE plot shows a flat pattern with no relative enrichment in either LREE or HREE (Fig. 8A). LILE are slightly enriched with respect to REE and HFSE, and show a strong Nb negative anomaly. Cazañas et al. (1998) concluded that there were at least two island arcs in the northeastern Caribbean domain from the late Danian to the middle Eocene. One calc-alkaline arc evolved as part of the main CVA, which is also found in the Dominican Republic and Puerto Rico (Cazañas et al., 1998 and references therein). The second one is a typical IAT arc, well represented in the rocks of eastern Cuba (Sierra Maestra arc). Thus, the volcanism in the Sierra Maestra was independent from the other areas of the Caribbean domain with similar characteristic to that of the Kermadec arc in the SW Pacific (Fig. 8B; Ewart et al., 1977; Ewart and Hawkesworth, 1987).

Geochemistry of the granitoids

Granitoid intrusions of the Sierra Maestra have been studied by various authors with data summarized in Eguipko et al. (1984), Iturralde-Vinent (1996b), Rodríguez-Crombet et al. (1997), Kysar Mattietti (2001) and Rojas-Agramonte et al. (2004). These rocks define several massifs from west to east, namely Turquino, Peladero, Nima-Nima and Daiquirí (Fig. 2B). Granitoid clasts occur in the Camarones Conglomerate, showing that the uppermost levels of the granitoid bodies experienced erosion during the late Eocene. The general mineralogical composition of the granitoids includes magmatic minerals such as quartz, amphibole, plagioclase, biotite, sphene, zircon, apatite, and secondary minerals such as chlorite and epidote.

Three distinct magmatic associations can be recognized in the granitoid suite of the Sierra Maestra: (1) a gabbro-tonalite association; (2) a tonalite-granodiorite association (Eguipko et al., 1984); and (3) a monzodiorite association (Rodríguez-Crombet et al., 1997). Based on their major element compositions these granitoids can be classified as low- to medium-K, calc-alkaline, I-type intrusives (Eguipko et al., 1984).

In this section all granitoids have a well preserved igneous texture and consist predominantly of well zoned and twinned plagioclase and undulatory quartz with variable proportions of hornblende and/or biotite. Plagioclase generally has a euhedral to subhedral calcic core and anhedral more sodic overgrowth rims. Minor to moderate sericitization of plagioclase is ubiquitous; hornblende is sometimes altered to biotite and/or chlorite, and formation of secondary epidote is minor to moderate (Rojas-Agramonte et al., 2004).

Most granitoids of the Sierra Maestra plot in the fields of tonalite or trondhjemite in the An-Ab-Or diagram, whereas pebbles from the Camarones Conglomerate are predominantly trondhjemitic in composition (Rojas-Agramonte et al., 2004). The calc-alkaline nature of these rocks is well displayed in the AFM-diagram (Rojas-Agramonte et al., 2004) and the Na_2O- and K_2O-contents clearly identify these rocks as I-type granitoids (Hine et al., 1978). SiO_2-contents range from 59 to 73 wt.%, whereas the granitoid pebbles from the Camarones Formation show two distinct groups with 65–66 and

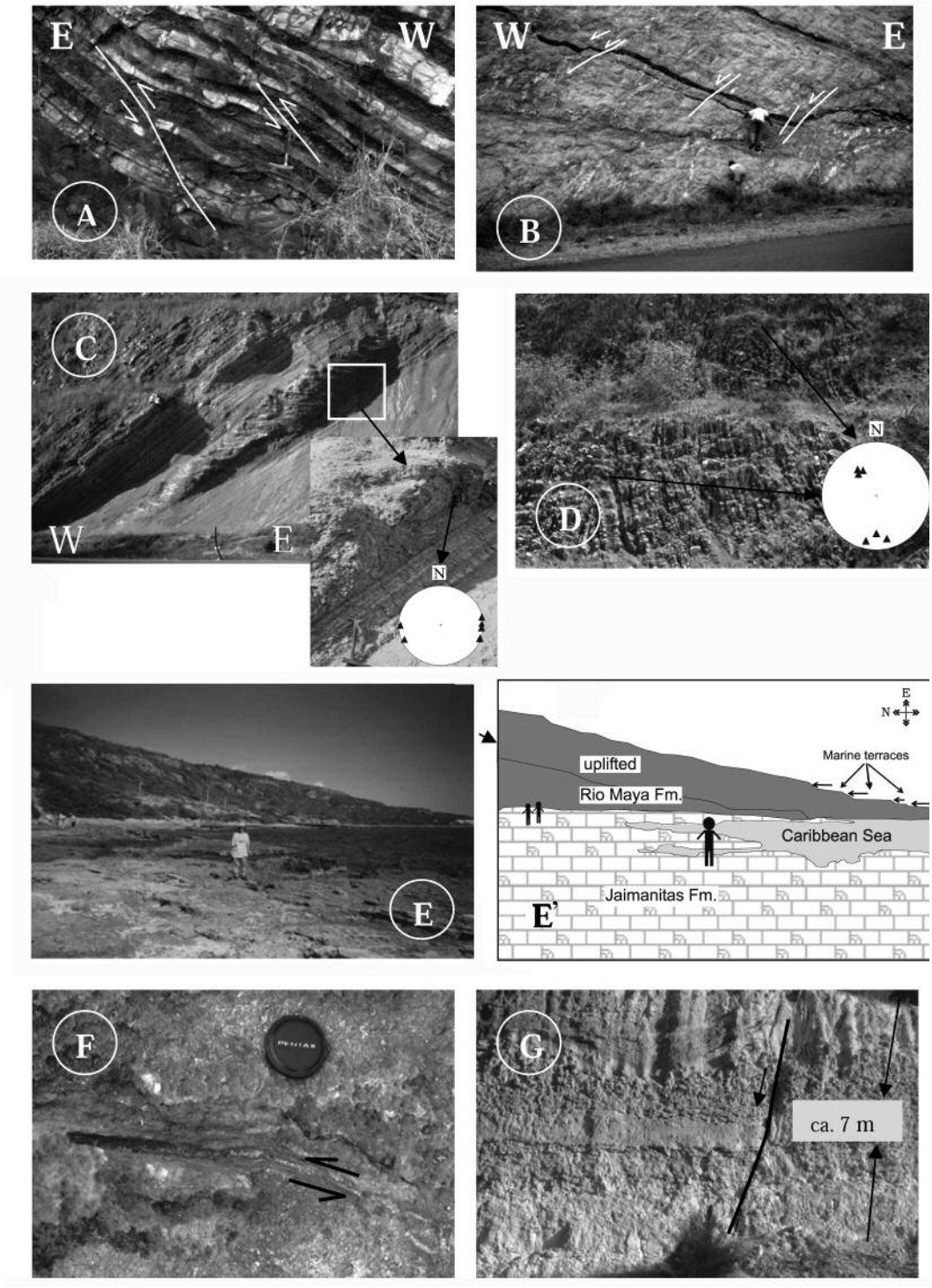

FIGURE 7 | **A) Reverse fault and thrust resulting from N–S compression and found in rocks of the El Cobre Group to the north of the Gran Piedra block. B) Mafic dyke intruding granitoid massif in central Sierra Maestra close to the coast; several normal faults cut the dyke. C) Folding in rocks of the San Luis Formation to the north of La Gran Piedra (outcrop is almost 10 metres high), with rectangle showing location of close-up view. Close up shows fold above thrust in sediments of San Luis Formation Inset shows stereoplot with orientation of fold axes. D) Open to isoclinals folds in Pilón area; inset stereoplot shows orientation of fold axes; the sequence is ca. 5 m thick. E and E') View looking at the southeastern part of the Gran Piedra block. Terraces exposed in Rio Maya Formation. Person 1.65 m tall. F) Extensional vein reactivated as sinistral strike-slip fault due to NE-SW compression. Small-scale releasing bend can also be observed. G) Normal fault within La Cruz Formation to the east of Santiago de Cuba in the Santiago Basin.**

74–77 % SiO_2. Harker diagrams show a positive correlation of most major oxides, suggesting a possible common parental magma (Kysar Mattietti et al., 2001; Rojas-Agramonte et al., 2004). Only the Camarones pebbles show some deviating patterns, suggesting either significant fractionation or a different magma source. SiO_2 plotted against (Na_2O+K_2O) displays the subalkaline nature, and SiO_2 plotted against K_2O exhibits the low to medium-K character, typical of intra-oceanic island-arc plutonic rocks, also known as M-type granites (Pitcher, 1983) such as in Puerto Rico, The Virgin Islands (Lidiak and Jolly, 1996), the Aleutians (Mahlburg-Kay and Kay, 1994), the Izu-Bonin-Mariana arc (Kawate and Arima, 1998), and the New Britain island arc (Whalen, 1985).

Immobile trace elements such as Nb and Y classify the Sierra Maestra granitoids as volcanic arc granites (Fig. 8C; Rojas-Agramonte et al., 2004). Enrichment in highly incompatible elements (Rb, Ba, Th, U, K), slight elevation in Sr and depletion in Nb and Ta are typical of subduction-related magmatism (Brown et al., 1984; Kawate and Arima, 1998). Although some Rb- and Ba-values may not be primary due to some post-crystallization alteration, the general trace element distribution underlines the intra-oceanic origin of these rocks (Kysar Mattietti, 2001; Rojas-Agramonte et al., 2004).

Compared with the primitive mantle (Sun and McDonough, 1989), rare earth element (REE) patterns are flat to moderately enriched in LREE with La_N/Yb_N ratios slightly varying from massif to massif (Fig. 8D). The highest $(La/Yb)_N$ ratio is found in granitoids of the Turquino and Peladero Massifs, and in pebbles of the Camarones Conglomerate; the lowest in the Nima-Nima and Daiquirí Massifs. Granitoids of the Nima-Nima and Daiquirí massifs show flat REE patterns. Eu shows no or moderate negative anomalies that tend to correlate with high SiO_2-contents, but in some cases such as in the Nima-Nima and Daiquirí Massifs there are also slightly positive Eu anomalies which correlate with high plagioclase contents such as in the sample from the Nima-Nima massif. The REE patterns for the Peladero granitoids are distinctly U-shaped, suggesting depletion of the middle REE due to fractionation of amphibole and/or apatite (Kobayashi and Nakamura, 2001). This feature is also apparent, but less pronounced, in the other granitoids.

Flat REE-patterns with variable slight (mainly negative) Eu-anomalies are also characteristic of basaltic to dacitic volcanic rocks of the Palaeocene to Middle Eocene El Cobre Group in the Sierra Maestra (Fig. 8A and 8D), as well as in Upper Cretaceous to Eocene magmatic rocks of the Dominican Cordillera (Lewis et al., 2002), Puerto Rico and The Lesser Antilles arc, and in the Izu-Bonin-Mariana arc of the West Pacific (White and Patchett, 1984; Kawate and Arima, 1998) and in M-type granitoids of the New Britain arc of Papua New Guinea (Whalen, 1985). The above petrographic and geochemical features, in particular the flat to slightly enriched REE patterns, suggest that the Sierra Maestra granitoids were produced by fractional crystallization of a mantle-derived basaltic magma (Rojas-Agramonte et al., 2004).

GEOCHRONOLOGY

Previous radiometric dating on these plutons was carried out in the former USSR, using the K/Ar method (Iturralde-Vinent, 1996b; Rodríguez-Crombet et al., 1997; Table 1, see Appendix). Kysar et al. (1998) and Mattietti-Kysar (1999) reported precise conventional U-Pb zircon ages from these plutons with ages ranging from 46 to 56 Ma (Table 1, see Appendix). From these ages Mattietti-Kysar (1999) ascribed the magmatic evolution of the PVA to two distinct magmatic episodes, separated from each other by 6–10 m.y. Kysar Mattietti et al. (2001) also reported whole-rock lead isotopic data for various igneous rocks of the PVA in the Sierra Maestra and postulated the existence of a single magma source from the homogeneous nature of these data.

U-Pb SHRIMP zircon ages

Single zircons from five granitoid samples of the Sierra Maestra PVA were analyzed on SHRIMP by Rojas-Agramonte et al. (2004), the results are summarized in Table 1 (see Appendix). Zircons of a trondhjemite sample from the Turquino Massif are colourless to light yellow, long-prismatic and perfectly euhedral. Three spot analyses from different zircons in this sample yielded concordant results with a mean $^{206}Pb/^{238}U$ age of 60.2 ± 2.6 Ma. A tonalite sample from the same massif and of similar composition also contains clear, euhedral zircons of which eight spot analyses provided a mean $^{206}Pb/^{238}U$ age of 55.4 ± 0.7 Ma, which is identical to a conventional U-Pb zircon age of 56 Ma (no error given) for the Turquino granitoid (Mattietti-Kysar, 1999). These are the oldest ages of our granitoid suites, documenting Palaeocene plutonic activity of the PVA during deposition of the El Cobre Group volcanic and sedimentary rocks.

A tonalite sample from the Peladero Massif also contains a homogeneous population of clear, euhedral zircons of magmatic origin, and seven spot analyses give a $^{206}Pb/^{238}U$ age of 48.2 ± 0.4 Ma, probably defining the termination of plutonic activity during deposition of the Caney Formation in the early middle Eocene.

Two tonalite samples were dated from the Nima-Nima Massif SW of Santiago de Cuba. The zircons are again

clear, transparent and idiomorphic with characteristic magmatic growth patterns as seen in CL images. Eight spot analyses of zircons from one sample give a $^{206}Pb/^{238}U$ age of 50.5 ± 0.5 Ma, identical to the age of 50.1 ± 0.5 Ma for six grains in the other sample from the same massif.

Zircons from a tonalite sample of the Daiquirí Massif exposed SE of Santiago de Cuba are exceptionally clear, colourless to light yellow and perfectly euhedral with well developed magmatic oscillatory zoning. Analysis of five grains yielded a combined mean $^{206}Pb/^{238}U$ age of 50.1 ± 0.5 Ma, which is identical to conventional U-Pb zircon ages of 49.8 ± 0.3 and 50.2 ± 0.1 Ma reported by Kysar et al. (1998). Interestingly, one additional grain of identical morphology and internal structure produced a much higher concordant $^{206}Pb/^{238}U$ age of 310.8 ± 3.4 Ma. We do not exclude the possibility that this grain is exotic and may reflect laboratory contamination during sample preparation, but the morphological similarity of this zircon grain with respect to the others argues against this interpretation. If the ~311 Ma zircon is indeed from sample CU-5 then the source region of this granite contains late Carboniferous crustal material and the PVA may then not be entirely intra-oceanic. It may be no coincidence that the anomalously high K-Ar age of 76 ± 3.8 Ma for a gabbro as reported by Rodríguez-Crombet et al. (1997) also comes from the Daiquirí Massif, suggesting the potential presence of pre-Palaeocene crust in the root zone of the Sierra Maestra PVA.

$^{40}Ar/^{39}Ar$ Geochronology

Two multigrain biotite samples from the Peladero and Nima-Nima massifs were dated using the $^{40}Ar/^{39}Ar$ laser

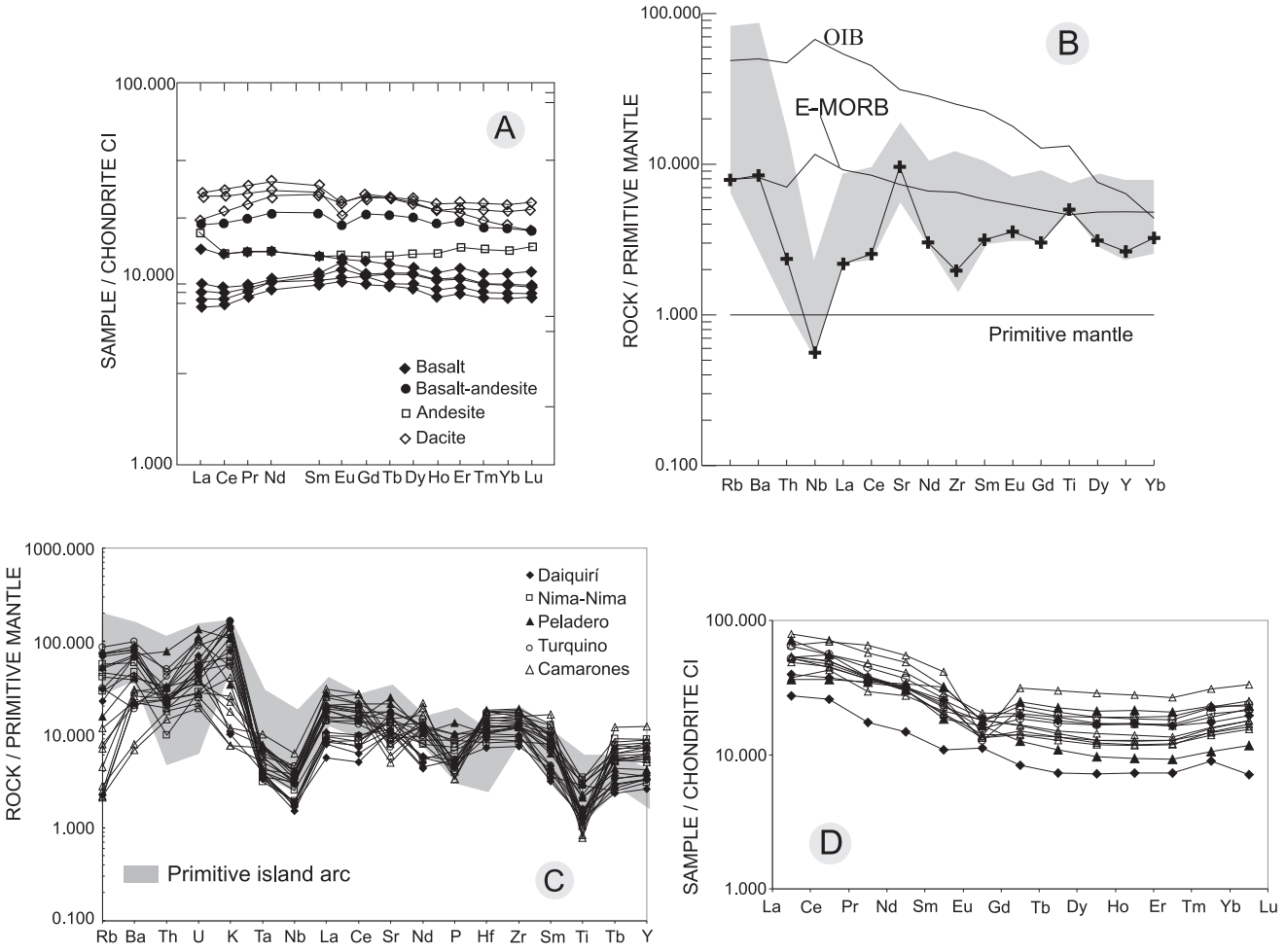

FIGURE 8 **A) REE diagram, normalized to chondritic values, for the volcanic rocks from the Lower and Intermediate Sequences of El Cobre Group (Cazañas et al., 1998). B) Comparison of the trace elements (shadowed area) from the Lower and Intermediate Sequences of El Cobre Group with those from the Kermadec primitive island arc (crosses; Cazañas et al., 1998). C). Primitive mantle-normalized multi-element diagram showing field of primitive island and continental arcs (Brown et al., 1984) and Sierra Maestra granitoids. Legend to the right shows sample number for the different granitoids (after Rojas-Agramonte et al., 2004). D) Chondrite-normalized REE patterns for Sierra Maestra granitoids. Normalizing values from Sun and McDonough (1989; after Rojas-Agramonte et al., 2004). Symbols as in Fig. 8C.**

ablation method. Analytical techniques follow those of Liu et al. (2001). The results are shown in Table 2 (see Appendix) and are portrayed as age spectra in Fig. 9. Both biotite samples show some variability in low-energy increments of the experiment, reflecting minor disturbance of the Ar isotopic system subsequent to initial closure. Intermediate to high energy steps of the experiment together constitute more than 70% of the ^{39}Ar released and yielded well-defined plateau ages of 50 ± 2 and 54 ± 4 Ma (Fig. 9). These ages are interpreted to record cooling through ca. 300ºC, the appropriate argon closure temperature of biotite (MacDougall and Harrison, 1999).

Fission track ages (FT)

Mineral concentrates from the Turquino, Peladero, Nima-Nima and Daiquirí massif were obtained using standard heavy liquid and magnetic separation techniques. Zircon FT dating was carried out at the Institute of Geology and Palaeontology, Graz University, using the external detector method as described in Bojar et al. (1998). The analytical results are shown in Table 3 (see Appendix). For apatite FT dating the grain population method was used in the laboratory of Salzburg University (Hejl, 1997). Samples were dated using the population method (Wagner, 1968; Wagner and Van den Haute, 1992). Zircon FT ages were determined for five samples and apatite FT ages for two samples. The zircons yielded older ages ranging from 32 ± 3 to 46 ± 4 Ma and are interpreted to reflect cooling through approximately 250 ± 50 °C (Tagami et al., 1996). The apatite FT ages are 31 ± 10 to 44 ± 13 Ma (Table 4, see Appendix), indicating fast cooling from 250 ± 50 °C to 110 ± 20 °C. Track length measurements show a bimodal distribution (Fig. 10A).

Figure 10B shows the cooling path modelling of the Nima-Nima granitoid, with a typical bimodal frequency distribution, related to stepwise cooling which has been modelled with a fission track age of 44 Ma. The model indicates fast cooling between 45 and 40 Ma, followed by a period of 30 Ma where almost no variation occurred in the temperature of the massif. We correlate final and fast cooling during the early Miocene (since 12 Ma) with activity along the OTWC and relate it to the onset of separation of the Hispaniolan arc from eastern Cuba.

GEOBAROMETRY

The chemical composition of rock-forming minerals from five granitoids samples has been determined by electron microprobe in order to assess the pressure and temperature conditions during solidification of various sites during granitoid intrusion (Table 5, see Appendix; Fig. 2). Pressures were calculated using the hornblende geobarometer of Schmidt (1992), modified by Ague (1997). For a temperature estimate the geothermometer of Holland and Blundy (1994) was applied. In both cases we used the PET software (Dachs, 1998). As described in the section Geochemistry of the Granitoids the main mineral composition of these samples is zoned and twinned plagioclase, undulous quartz, biotite, hornblende and minor K-feldspar.

Good temperature estimates were obtained for the granitoids located in the eastern part of the Sierra Maestra (Daiquirí and Nima-Nima Massifs), because their chemical composition is more appropriate than those located in the western part. Hornblende in these two granitoids is Mg-rich, whereas hornblende from the Turquino Massif in the western part is iron-rich (Fig. 11). Temperature estimates for these granitoids in the eastern part show a wide range from 600 to 900°C. These data may reflect the crystallization temperature of hornblende and, possibly, also of hornblende overgrowth that was found on some crystals. In some samples of the Daiquirí Massif hornblende cores have low-alumina contents, possibly indicating relicts of an older amphibole generation. Pressure estimates for four samples suggest 1.8–3 kbar, which corresponds to a depth of ca. 4.5–8 km (Fig. 12).

PALAEOSTRESS ANALYSIS

A palaeostress analysis was carried out along the southern slopes of the Sierra Maestra mountain range by Rojas-Agramonte et al. (submitted). This palaeostress study was applied in the Sierra Maestra in order to determine the tectonic evolution of this area and to determine the transition from arc-continent collision to transform motion during Tertiary times in this region. Outcrop-scale faults with slip lines (striae), veins and folds were mea-

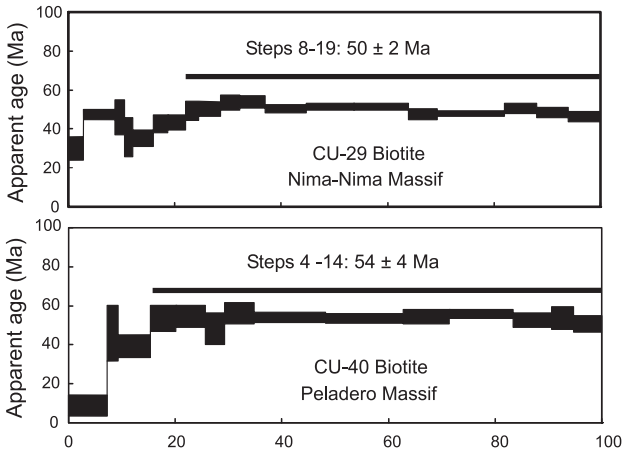

FIGURE 9 | **^{40}Ar/^{39}Ar release spectra of biotite from granite intrusions in the Sierra Maestra.**

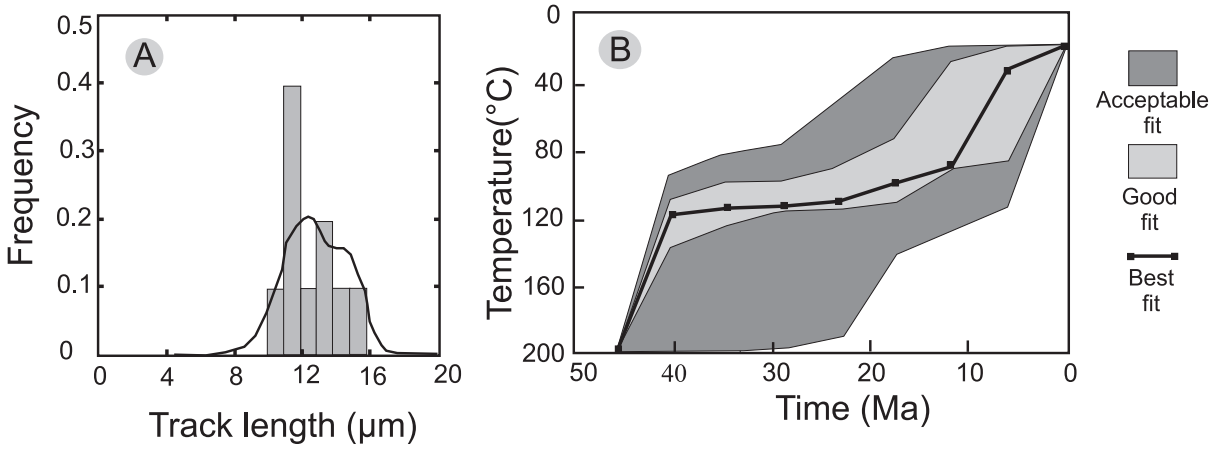

	Model	Data	Number	G.O.F.
Age (Ma)	36.2	44.1 ± 13.1	1	0.55
TL (mm)	12.9 ± 1.9	12.5 ± 1.5	10	0.99

FIGURE 10 | **Cooling path of granitoids from the Sierra Maestra. G.O.F: Goodness of fit.**

sured in volcanic rocks of the El Cobre Group, including the Pilón and Caney Fms and in granitoids, as well as in the middle to late Eocene rocks of the San Luis, Charco Redondo and Farallón Grande Fms. Six phases of deformation were recognized in the entire region (Rojas-Agramonte et al., submitted; Table 6, see Appendix). Deformations D_3 to D_6 are in agreement with a palaeostress study carried out on late Miocene to Quaternary formations in the southern Sierra Maestra (Rojas-Agramonte et al., 2005)

The first deformation phase (D_1) developed in an extensional tectonic environment and was accompanied by intrusion of andesitic and aplitic dykes and extensional veins filled with epidote, chlorite, quartz and, possibly, some filled with calcite. In the eastern part of the Sierra Maestra this phase is characterized by E–W and N–S extension found in andesitic volcanics and granitoid intrusions, whereas for the veins NW–SE, NNE–SSW to NE–SW and WNW–SSE extension is dominant. In the central Sierra Maestra appear N-trending synclines and anticlines due to E–W contraction (Fig. 6B). N–S-striking thrust faults also appear to be associated with this event.

The Gran Piedra block corresponds to an E–W extensional regime characterized by veins filled with epidote and chlorite and the intrusion of aplitic dykes. Felsic and aplitic dykes were emplaced during NNW–SSE extension. All these dykes and veins were subsequently reactivated and overprinted by reverse, normal and strike-slip faults.

Deformation phase D_2 is dominated by N–S compression, characterized by reverse faulting and folding. These faults locally reactivated many calcite-filled and, less so, epidote- and quartz-filled extensional veins. Dextral strike-slip faults also formed due to this compressional phase. We have also found quartz veins that were reactivated as sinistral strike-slip faults due to N–S compression. Reverse faults formed due to NE–SW compression are also associated with this phase as well as isoclinal folds. In some outcrops calcite fills extensional veins are due to E–W extension.

N–S compressional structures are numerous in the Gran Piedra block, and reverse faults and overthrusts were measured in rocks of the Charco Redondo and San Luis Fms. Overturned folds trending E–W also formed in rocks of the San Luis Fm. Epidote extensional veins were reactivated during this phase, and normal faults formed due to E–W extension as well as NNW-striking dextral strike-slip faults due to NNE–SSW compression.

Deformation phase D_3 (N–S extension) produced mainly S-dipping normal faults that locally appear to overprint structures formed during the D_2 N–S compression event and also surfaces that were reactivated as normal faults and were first filled by calcite. In Gran Piedra this deformation also produced E–W-striking normal faults which overprint structures of the D_2 N–S compressional event. Calcite-filled veins were reactivated as normal faults during this phase.

NE–SW compression (Deformation phase D_4) produced WNW and NNE-oriented sinistral strike-slip faults that overprinted normal faults or reactivated older surfaces. N- to NNE-oriented dextral strike-slip faults also reactivated older fractures (veins filled by calcite). The

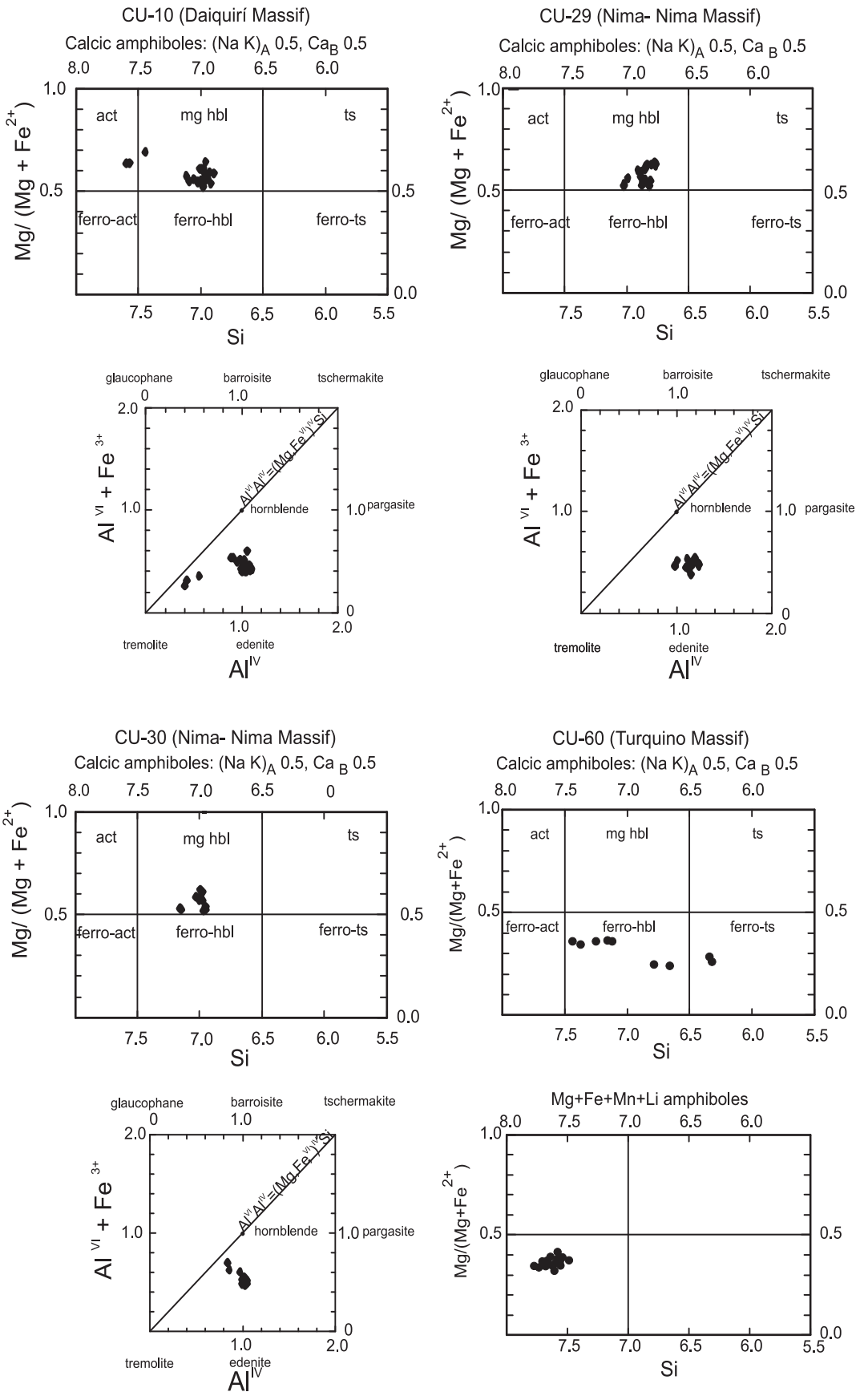

FIGURE 11 | **Chemical composition of hornblende from 4 samples in three granitoids massifs, determined by electron microprobe. Hornblendes from Daiquiri and Nima-Nima Massifs are Mg-rich, whereas hornblendes from Turquino Massif are Fe-rich. The lower alumina concentration in hornblende of sample CU-10 corresponds to 3 core measurements, suggesting that these minerals cores represent an older hornblende generation.**

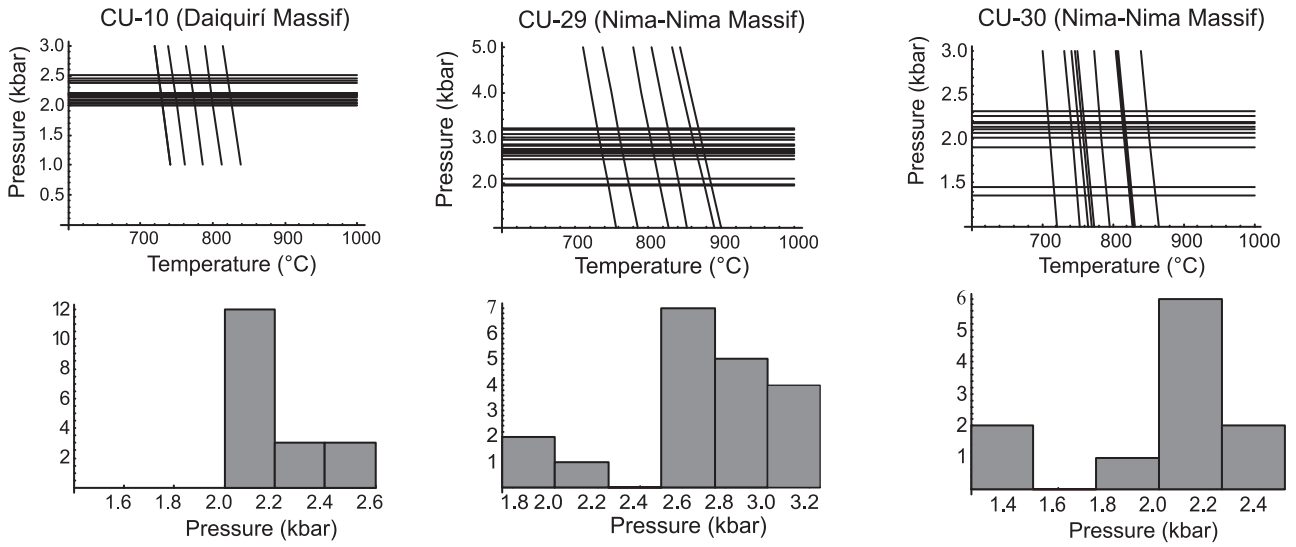

FIGURE 12 | **Calculated pressures and temperatures for emplacement of granitoids in the Daiquirí and Nima-Nima Massifs. Data were calculated from hornblende and plagioclase compositions of Table 1. Samples CU-29 and CU-30 show lower pressure corresponding to rim composition of hornblende. Horizontal lines represent aluminium-in-hornblende barometer and vertical lines hornblende + plagioclase thermometer.**

formation of dextral strike-slip faults was followed by the formation of normal faults due to NW–SE extension. Reverse faults are also associated with this phase.

In the Gran Piedra block the D_4 event produced dextral, N-oriented strike-slip faults due to NE–SW compression, which also overprinted NNE-striking normal faults. Karst-filled cracks formed due to NW–SE extension and are also related to this event.

During the deformation phase D_5, E–W striking reverse faults overprinted normal faults that formed due to N–S extension. NW–SE compression produced NNW-oriented sinistral strike-slip faults in the Gran Piedra and appears to overprint normal faults formed due to E–W extension. Karst-filled fractures (filled with red soil and sedimentary breccia) formed due to NE–SW extension.

Structures of the last phase (D_6) appear to overprint all older features and comprise dextral, sinistral and reverse faults that formed due to E–W to nearly WNW–ESE compression. Sinistral faults appear to overprint reverse faults due to WNW–ESE compression; at the same time sinistral faults appear to reactivate chlorite- and calcite-filled veins. Reverse faults that formed due to E–W compression also reactivated chlorite-filled veins. As a consequence of this major compressional event, normal faults formed due to N–S extension. NW- to WNW-oriented sinistral strike-slip faults are dominant in the Gran Piedra block.

DISCUSSION

The tectonic evolution of the Sierra Maestra provides evidence for an Eocene to Miocene transition from regional N- to NE-directed compression to left-lateral strike-slip deformation along the OTWC. This transition is monitored by the different deformation phases discussed above and described in detail by Rojas-Agramonte et al. (submitted). The architecture of the Sierra Maestra Mountains reveals an overall antiformal structure, which includes a monocline (e.g., Fig. 5, cross-sections B–B´, C–C´) with its limb dipping to the north. The southern flank of this structure is now exposed in Hispaniola after Neogene disruption of these two regions (Iturralde-Vinent, 1996a). Anticline formation is likely to have been contemporaneous with granitoid intrusion and deposition of siliciclastic sediments along the northern margin of the anticline.

The Tertiary evolution of the Sierra Maestra can be summarized in terms of six distinct phases of deformation (Table 6, see Appendix). The available data (Rojas-Agramonte, 2003; Rojas-Agramonte et al., 2004, 2005) are compatible with recent tectonic models (Leroy et al., 2000; Pindell and Kennan, 2001) and allow a more detailed insight as follows and as illustrated in Fig. 13.

D_1: Late Palaeocene to middle Eocene

The first phase of deformation includes a set of subparallel, N-striking subvertical basalt/andesite dykes that monitor N–S shortening and E–W extension. These may have formed during the waning phases of PVA magmatic activity since some dykes cut Eocene tuffs of the Pilón Fm. These dykes indicate N–S shortening (within present-day coordinates) during subduction and a compressive setting for the PVA. The granitoids form stock-like plutons, and it is not clear whether they intruded in a compressive tectonic environment. These granitoids were

emplaced 60 to 48 Ma ago and have a tonalitic to trondhjemitic composition. The oldest ages of the granitoid suites are 60.2 ± 2.6 and 55.4 ± 0.7 and suggest early Palaeocene plutonic activity for the PVA. $^{40}Ar/^{39}Ar$ ages for the Nima Nima and Peladero massifs are similar to the SRIMP ages for the same massifs.

During cooling, many epidote- and/or quartz-bearing veins formed with a preferred N–S orientation. These are similar in orientation to earlier dykes and, therefore, indicate continuous N–S compression during the middle Eocene. The youngest age of 48.2 ± 0.4 Ma probably defines the termination of plutonic activity during deposition of the Caney Fm in the early middle Eocene. Magmatism in the Sierra Maestra was continuous and lasted for about 10–12 million years as suggested by the uniform chemistry and similar zircon ages. This magmatism evolved from a single, though not necessarily chemically homogeneous, source (Rojas-Agramonte et al., 2004).

The rifting process in the Cayman trough predates the middle Eocene (Rosencrantz, 1990; Leroy, 1995). This rifting may have begun in the late Palaeocene to early Eocene if it correlates with rifting and extension associated with fissural volcanic activity in west-central Haiti (Pubellier et al., 2000 and references therein). This partially coincided with dyke intrusion and vein formation in the Sierra Maestra, since we already stated these two regions were part of the same crustal unit until the early Miocene. Pérez-Pérez and García-Delgado (1997) described several deep faults with sublatitudinal strike that originated after Palaeogene volcanism began in the Sierra Maestra. These faults were interpreted to form conduits for fissure volcanoes (Pérez-Pérez and García-Delgado, 1997) and could be related to the same process in Haiti. Rojas-Agramonte et al. (submitted) suggested that the Sierra Maestra remained unified with Hispaniola until the late Palaeocene when it was separated from mainland Cuba (Fig. 13A). These authors proposed that the PVA in the Sierra Maestra formed along strike of the subduction zone and may have had another orientation than today. Later, during the middle Eocene, mainland Cuba collided with the Bahamas platform, thus forming the Cuban Orogen (Fig. 13B).

D_2: Middle Eocene to early Oligocene

Collision of the Cuban Orogen with the Bahamas platform (North American plate) in the middle Eocene (Iturralde-Vinent, 1994, 1998) coincided with the end of magmatic activity in the Sierra Maestra. This event is also dated by the oldest zircon FT age of 44 ± 4 Ma, indicating the beginning of exhumation of the granitoid suite.

The Nipe-Guacanayabo fault system (Fig. 13B) accommodated the northeastward relative motion of the Caribbean plate; this is compatible with N–S shortening. Uplift in the Sierra Maestra began, and deposition of coarse clastic sediments commenced in the late middle Eocene (Farallón Grande Fm) and continued through the late Eocene (Camarones Fm). Deposition of breccias of the Farallón Grande Fm in the west suggests steeper slopes in this area than in the central and eastern Sierra Maestra for the middle to late Eocene, suggesting an eastward migration of surface uplift. In the central eastern Sierra Maestra the San Luis Fm begins with fine clastic sediments, passing into the coarse clastic Camarones Fm to the east. Lewis and Straczek (1955) suggested that deposition of the San Luis and Camarones Fms was due to a crescendo in uplift of a land mass to the south. The most differentiated, uppermost parts of the granitoid plutons were already exposed prior to the late Eocene and provided detritus for sediments of the Upper Eocene Camarones Fm.

Approximately N–S compression (D_2) within present-day coordinates is constrained by the formation of conjugate Mohr shear sets, dextral NW-striking faults and NE-striking dextral faults (Rojas-Agramonte et al., submitted). This event is likely to have been related to the formation of E–W oriented thrusts and coincides with external stress conditions, which are necessary to form E-trending folds, constituting together a set of collisional structures (Rojas-Agramonte et al., submitted). The large-scale structure also displays weak, E- to ESE trending folds. These large-scale folds also affected the Camarones Fm (Fig. 5, cross-section D–D´) and are likely to have formed during the same stress conditions as N-directed local thrusts. This event (D_2) most likely began in the middle to late Eocene, when uplift in the Sierra Maestra began, and most deformation was terminated in the early Oligocene after deposition of the Camarones Fm (Fig. 3, cross-section D-D´ Fig. 5), as indicated by the younger zircon FT age of 32 ± 3 Ma.

A reorientation of the Caribbean plate stress field from mainly NE–SW to dominantly E–W occurred in the early Oligocene (Iturralde-Vinent and Macphee, 1999). For this reason the Eastern Cuban microplate could not continue its northeastward movement, and the Nipe-Guacanayabo fault system was abandoned. A deformation front developed where the Oriente Fault is now located. The Eocene–Oligocene transition was a time of general uplift and erosion, and the Farallón Grande Fm to the west and Camarones Fm to the east (Figs. 2A and 3) witnessed this process by receiving coarse clastic sediments from the uplifted areas in the Sierra Maestra. The overall shortening is relatively minor as the large open folds and subordinate offsets on outcrop-scale reverse and thrust faults indicate. Shortening in the Sierra Maestra was accommodated by N–S thrusting and ca. E–W trending

folds, propagating north to northeastward (Rojas-Agramonte et al., submitted).

Uplift in the Sierra Maestra was the result of a combination of tectonic and thermal processes, namely collision of the Caribbean and North American plates in the middle Eocene and initiation and further development of the Oriente Transform Fault in the late Oligocene. The Sierra Maestra did not directly collide with the Bahamas Platform. Nevertheless, we argue that collision between the Cuban Orogen and the Bahamas Platform indirectly caused deformation in the Sierra Maestra. Subsequently, due to sinistral motion along the OTWC, the Sierra Maestra continued to be uplifted, and this process is still taking place (Rojas-Agramonte et al., 2005). Uplift was the result of shortening, and the active collision front proceeded to eastern Cuba, and the Sierra Maestra island arc docked with the Cuban orogen (Fig. 13B).

D_3: Late Oligocene to early Miocene

Compressive structures were overprinted by N–S extensional structures (D_3). Rojas-Agramonte et al., submitted interpreted the numerous local normal faults to have resulted from a major S–directed detachment system. This event most likely occurred during the late Oligocene to early Miocene. Iturralde-Vinent (1998) already described this set of normal faults for the Oligocene.

In the late Oligocene the ECM became attached to the North American plate, the plate boundary jumped to the Oriente fault (Iturralde-Vinent and Gahagan, 2002), and a regional plate reorganization occurred (Leroy et al., 2000). During the early middle Miocene the Caribbean region showed the effect of disruption of Cuba and Hispaniola by oblique transtension (Fig. 13C), likely due to oblique spreading in the Cayman trough. Apatite fission track ages record the onset of separation of the Hispaniolan arc assemblage from eastern Cuba in the early Miocene at about 12 Ma ago. Localized extension occurred during this phase, and grabens, pull-apart basins and trenches began to form (Iturralde-Vinent and Macphee, 1999).

D_4–D_6: Early middle Miocene to Recent

Further evolution of the Sierra Maestra mountain range is related to initiation of transcurrent motion along the North Caribbean Transform Fault (D_4–D_6). The OTWC as the leading master fault of the North Caribbean transform system strikes approximately E–W. This fault is primarily responsible for the formation of the steep topographic gradient along the southern Cuban coast (Fig. 2A). Quaternary to Recent structures in the sea indicate compression in the east and extension in the west (Rojas-Agramonte et al., 2005).

Subsequent sinistral shearing along E–W striking faults is related to deformation phase D_4, implying ca. NW–SE maximum principal stresses. This event can be related to the main displacement along the OTWC, since corresponding faults were detected only close to the coast. Faults have the orientation and the en-échelon arrangement of Riedel shears, which generally form along wrench corridors (e.g. Mandl, 1988). This phase D_4 reflects pure sinistral transform motion (Fig. 13D). Later, the NE-ward indentation of the Beata ridge, an oceanic plateau, resulted in SW-vergent deformation in Hispaniola (Leroy et al., 2000).

The final deformation is characterized by dextral reactivation of WNW-oriented strike-slip faults in the Gran Piedra block, which may have formed at the same time as a few dextral E–W oriented strike-slip faults in the Sierra Maestra block. These faults can be explained by shear reversal along the OTWC, with mainly dextral transpressive displacement (Rojas-Agramonte et al., submitted). This event may also have been responsible for a clockwise rotation of the Gran Piedra block and initial formation of the Santiago deformed belt to the south of the Santiago basin (Fig. 2A). This belt comprises several thrust sheets, which indicate the generally convergent nature of this sector of the OTWC. This structure shows clear evidence of compression and probably existed since the late Pliocene (Calais et al., 1998).

Indentation of the Beata ridge resulted in fan-like extrusions in front of the indenter (Fig. 13E). This may have resulted in a dextral short-lived shear reversal along the Oriente fault (Rojas-Agramonte et al., submitted). GPS measurements show that present-day motion along the OTWC is almost parallel to the strike of the fault (Mann et al., 2002). From the middle Miocene to the present, motion and associated deformation have increased significantly. The northern boundary of the Caribbean plate is characterized by intense transpressive deformation resulting in ca. E–W to ENE–WSW compression that is still active today (Rojas-Agramonte et al., 2005 and references therein).

The sequence of deformation from D_4 to D_6 suggests a reversal of motion. D_4 indicates dextral displacement along the E–W striking OTWC, whereas D_5 reveals sinistral displacement, which later changed to nearly E–W compression. The question arises whether there is any supporting evidence for shear reversal along the OTWC. The final E–W compression (D_6) is in accordance with present-day transform motion as indicated by GPS data (Moreno et al., 2002; Mann et al., 2002). Transpression in the southern Sierra Maestra was distributed mainly between strike-slip faults trending almost parallel to the coast, whereas transtension occurred between NE-striking normal faults.

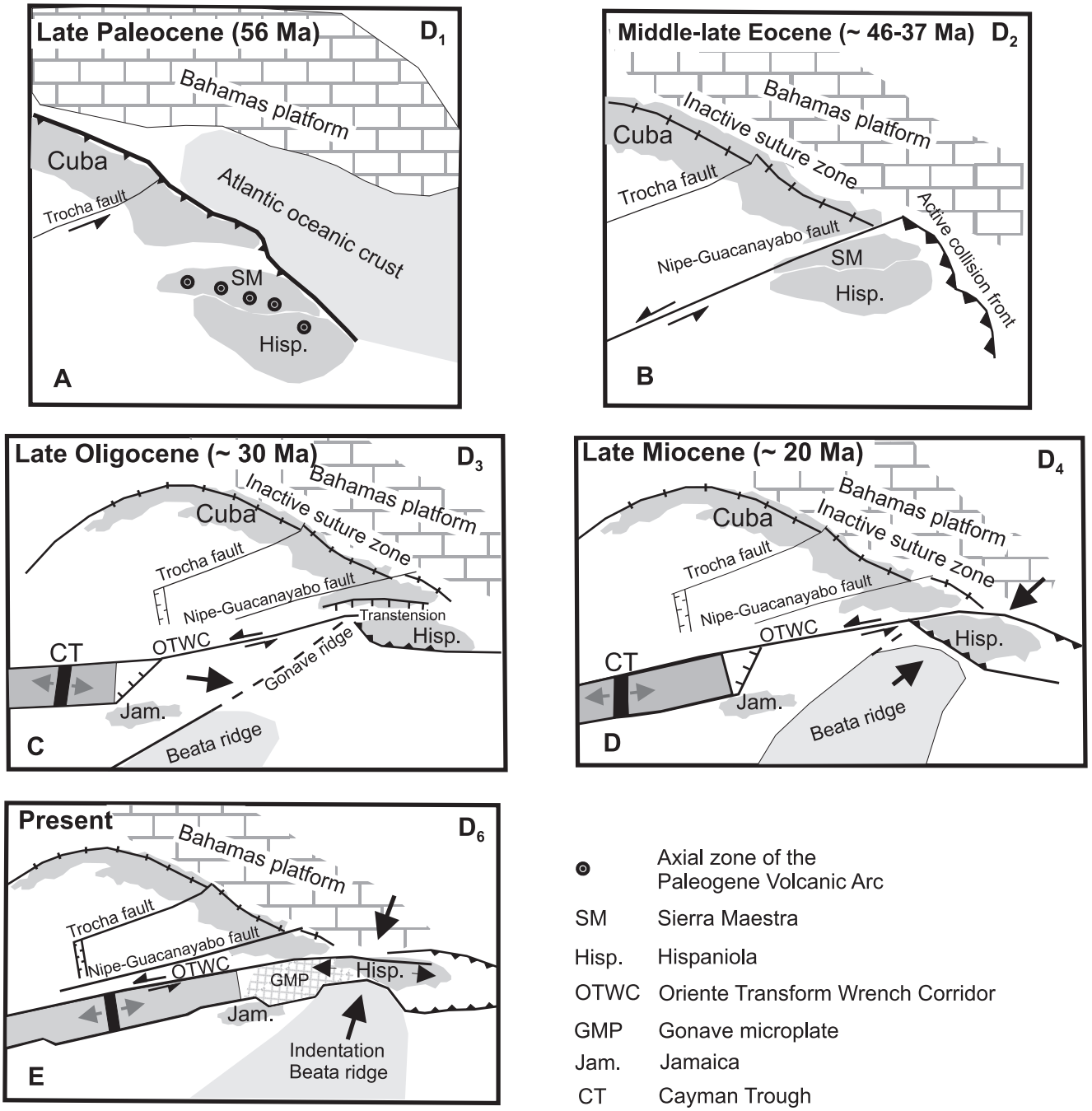

FIGURE 13 | **Tectonic evolution model of the northeastern Caribbean, from Palaeocene to Recent (after Rojas-Agramonte et al., submitted).**

CONCLUSIONS

Palaeogene volcanism, at least as it appears in the lower part of the El Cobre Group in the Sierra Maestra, originated in an island arc setting. El Cobre Group is a typical low-K IAT that is similar to other Caribbean arc sequences (Cazañas et al., 1998). The Sierra Maestra arc presents geochemical characteristics similar to that of the Kermadec arc in the SW Pacific. During the final stages of arc magmatism the Palaeogene Volcanic Arc sequences were intruded by tonalitic to trondhjemitic granitoids emplaced 60 to 48 Ma ago at pressures of 1.8-3 kbar and corresponding to depths of 4.5 to 8 km. Geochemical features characterize these rocks as typical subduction-related granitoids as found worldwide in intra-oceanic arcs, and they probably formed through fractional crystallization of mantle-derived low- to medium-K basalt. ^{39}Ar-^{40}Ar biotite ages on these granitoids are ca. 52–54 Ma and are interpreted to record cooling through ca. 300ºC. Zircon fission-track ages from 32 ± 3 to 46 ± 4 Ma reveal cool-

ing through ca. 250 ± 50 °C, and apatite fission-track ages of 31 ± 10 and 44 ± 13 Ma reflect cooling through ca. 110 ± 20 °C. These data suggest fast cooling and exhumation after collisional processes in the Eocene.

The structure of the Sierra Maestra resulted from collision of the eastern Cuban microplate with the North American plate during Oligocene to Neogene initiation and activation of the North Caribbean Transform Fault in accordance with the tectonic evolution of the North Caribbean region. We suggest that the PVA was generated under compressive conditions during a N–S shortening regime in present-day coordinates. The overall structure is the formation of a large orogen-wide anticline, which was modified by folds, reverse folds and thrust faults. Anticline formation is likely to have been contemporaneous with granitoid intrusion and deposition of siliciclastic sediments along the northern margin of the anticline. Apatite and zircon fission track data yield ages ranging from 46 ± 4 to 32 ± 3 Ma and indicate uplift in Eocene to Oligocene times. Coarse clastic sediments were deposited between the middle and late Eocene with clast provenance from the uplifted areas in the Sierra Maestra.

The North Caribbean transform fault modified the overall structure of the Sierra Maestra by wrenching, beginning in the Miocene and determining the present southern slope of the mountain range. The granitoid plutons were affected by normal and strike-slip faults, which are often located at the interface between granites and stronger country rocks. This is obviously the reason why granitoid massifs are now exposed close to the coast because these normal and strike-slip faults are part of the Oriente Transform Wrench Corridor, which cuts through the former central axis of the island arc system.

Finally, the kinematics of Sierra Maestra deformation can be attributed to a combination of oblique convergence between the Caribbean and North American plates and eastward escape of the Caribbean plate along a left-lateral strike-slip fault system after northeastward attachment of the Eastern Cuban Microplate. The second deformation phase (D_2) reflects the period of northeastward attachment of the Eastern Cuban Microplate. The third deformation (D_3) records a period of transition between mainly compressive to transcurrent motions. Final cooling at ca. 12 Ma is related to movement along the OTWC, when it became a sinistral transform system. The OTWC exhibits a fault and fracture pattern which agrees with first motion solutions derived from earthquake focal mechanisms (Calais et al., 1998). The phases of deformation from D_4 to D_6 described above characterize the dynamics of the south-eastern Cuban coast at the leading edge of the North American plate during formation and development of the northern Caribbean Oriente Transform Wrench Corridor.

ACKNOWLEDGEMENTS

Y. Rojas-Agramonte acknowledges financial support through a fellowship of the Austrian Academic Exchange Service (ÖAD). We thank Dr. Iturralde-Vinent for encouragement in writing the manuscript. We also acknowledge useful comments and the correction of the manuscript by Prof. Alfred Kröner. Thanks are due to Drs. Edgar Dachs, Gertrude Friedl and Dan Topa for assistance during analytical work and to the staff of the SHRIMP laboratory in Beijing, especially Drs. Y. S. Wan and D. Y. Liu. This is TSRC contribution No. 307 and a contribution to IGCP-Project 433 (Caribbean Plate Tectonics).

REFERENCES

Ague, J.J., 1997. Thermodynamic calculation of emplacement pressures for batholithic rocks, California: Implications for the aluminium-in-hornblende barometer. Geological Society of America Bulletin, 25, 563–566.

Alioshin, V., Burov, V., Eguipko, O., Eliseev, V., Sánchez Menéndez, F., Shelagurov, V., Koñujov, A., Varvarov, V., Lorkin, V., 1975, Sobre los resultados de los trabajos de levantamiento geológico y búsqueda en escala 1:100 000 ejecutados en las montañas de la Sierra Maestra, en la provincia de Santiago de Cuba y Granma (1972–75) Sierra Maestra nororiental. Instituto Nacional de Recursos Minerales, Ministry of Basic Industries, Havana, Cuba. Unpublished.

Bojar, A.V., Neubauer, F., Fritz, H., 1998. Cretaceous to Cenozoic thermal evolution of the southwestern South Carpathians: evidence from fission-track thermochronology. Tectonophysics, 297, 229–249.

Brown, G.C., Thorpe, R.S., Webb, P.C., 1984. The geochemical characteristics of granitoids in contrasting arcs and comments on magma sources. Journal of the Geological Society of London, 141, 413–426.

Cabrera-Castellanos, M., García-Delgado, D., Rojas-Agramonte, Y., Reyes-Pérez, C., Rivera-Alvarez, Z., 2003. Depósitos Cuaternarios al sur de la Sierra Maestra. V Congreso de Geología y Minería, Havana, Cuba, CD-ROM, ISBN-959-7117-11-8.

Calais, E., Perrot, J., Mercier de Lépinay, B., 1998. Strike-slip tectonics and seismicity along the northern Caribbean plate boundary from Cuba to Hispaniola. In: Dolan, J.F., Mann, P. (eds.). Active strike-slip and collisional tectonics of the northern Caribbean plate boundary zone. Boulder, Colorado, USA, Geological Society of America, Special Paper, 326, 125–141.

Case, J.T., Holcombe, L., Martin, R.G., 1984. Map of the geologic provinces in the Caribbean region. Geological Society of America, Memoir, 162, 1–30.

Cazañas, X., Proenza, J.A., Matietti Kysar, G., Lewis, J., Melgarejo, J.C., 1998. Rocas volcánicas de las series Inferior y Media del Grupo El Cobre en la Sierra Maestra (Cuba Oriental): volcanismo generado en un arco de islas tholeiítico. Acta Geologica Hispanica, 33, 57–74.

Coastal and Marine Geology Program: CMG InfoBank Atlas: Caribbean Sea region. http://walrus.wr.usgs.gov/infobank/gazette/html/bathymetry/cb.html

Dengo, G., Case, J.E., 1990, The Caribbean region. In: Dengo, G., Case, J.E. (eds.). The geology of North America. Boulder, Colorado, USA, Geological Society of America, Vol. H, 527 pp.

Dachs, E., 1998. PET. Petrological elementary tools for mathematica. Computers & Geosciences, 24, 219–235.

Draper, G., Barros, J.A., 1994. Cuba. In: Donovan, S.K., Jackson, T.A. (eds.). Caribbean geology: An introduction. Kingston, Jamaica, University of the West Indies Publishers Association, 65–86.

Eguipko, O., Sukar, K., Pavlov, V., Pérez, M., Gurbanov, A., Soto, T., 1984. Principales particularidades petroquímicas de los granitoides del eugeosinclinal cubano y sus formaciones. Ciencias de la Tierra y del Espacio, 9, 59–73.

Eguipko, O., Perez, M., 1976. Breves características petrográficas y petroquímicas de los principales tipos de rocas magmáticas en la parte central de la Sierra Maestra. Centro de Investigaciones Geológicas, Serie 1, 14 pp.

Ewart, A., Brothers, R.N., Mateen, A., 1977. An outline of the geology and geochemistry, and the possible petrogenetic evolution of the volcanic rocks of the Tonga-Kermadec-New Zealand Island Arc. Journal of Volcanology and Geothermal Research, 2, 205-270.

Ewart, A., Hawkesworth, C.J., 1987. The Pleistocene recent Tonga-Kermadec arc lava: interpretation of new isotopic and rare earth data in terms of a depleted source model. Journal of Petrology, 28, 495-530.

Hejl, E., 1997. "Cold spots" during the Cenozoic evolution of the Eastern Alps. Thermochronological interpretation of apatite fission-track data. Tectonophysics, 272, 159–172.

Hernández, J.R., González, R., Arteaga, F., 1989. Diferenciación estructuro-geomorfológica de la zona de sutura de la microplaca cubana con la Placa Caribe. La Habana, Editorial Academia, 48 pp.

Hernández-Santana, J.R., Díaz Díaz, J.L., Magaz García, A., Lilienberg, D.A., 1991. Evidencias morfoestructuro-geodinámicas del desplazamiento lateral siniestro de la zona de sutura interplacas de Bartlett. In: Morfotectónica de Cuba Oriental. Ed. Academia de Ciencias de Cuba, La Habana, 5–9.

Holland, T.J.B., Blundy, J. 1994. Non-ideal interactions in calcic amphiboles and their bearing on amphibole-plagioclase thermometr. Contributions to Mineralogy and Petrology, 116, 433–447.

Hine, R., Williams, I.S., Chappell, B., White, A.J.R., 1978. Contrasts between I- and S-type granitoids of the Osciusko Batholith. Journal of the Geological Society of Australia, 25, 19–234.

Hurford, A.J., Green, P.F., 1983. The zeta age calibration of fission-track dating. Isotope Geoscience, 1, 285-317.

Iturralde-Vinent, M.A., 1991. Deslizamientos y descensos del terreno en el flanco meridional de la Sierra Maestra, Cuba sudoriental. In: Morfotectónica de Cuba Oriental. Ed. Academia de Ciencias de Cuba, La Habana, 24–27.

Iturralde-Vinent, M.A., 1994. Cuban geology: A new plate tectonic synthesis. Journal of Petroleum Geology, 17, 39–70.

Iturralde-Vinent, M.A., 1996a. Introduction to Cuban geology and geophysics. In: Iturralde-Vinent, M.A. (ed.). Cuban ophiolites and volcanic arcs. Miami, Florida, USA, IGCP Project, 364, 3–35.

Iturralde-Vinent, M.A., 1996b. Cuba: El archipielago volcánico Paleoceno-Eoceno medio. In: Iturralde-Vinent, M.A. (ed.). Cuban ophiolites and volcanic arcs. Miami, Florida, USA, IGCP Project, 364, 231–246.

Iturralde-Vinent, M.A., 1998. Synopsis de la constitución geológica de Cuba. Acta Geologica Hispanica, 33, 9–56.

Iturralde-Vinent, M.A., 2003. The relationship between the ophiolites, the metamorphic terrains, the Cretaceous volcanic arcs and the Paleocene–Eocene volcanic arc. Field guide to a geological excursion to eastern Cuba. V Geological and mining congress. IGCP Project 433 Caribbean Plate Tectonics. Cuban Geological Society, 16 pp.

Iturralde-Vinent, M.A., Gahagan, L., 2002. Late Eocene to middle Miocene Tectonic evolution of the Caribbean: Some principles and their implications for plate tectonic modeling. In: Jackson, T.A. (ed.). Caribbean geology into the Third Millennium. Transactions of the Fifteenth Caribbean Geological Conference. Jamaica, Ed. Pear Tree Press Ltd., 47–62.

Iturralde-Vinent, M.A., Macphee, R.D.E., 1999. Paleogeography of the Caribbean region: implications for Cenozoic biogeography. Bulletin of the American Museum of Natural History, 238, 95 pp.

Jackson, T.A., Smith, T.E., 1979. Tectonic significance of basalts and dacites in the Wagwater belt, Jamaica. Geological Magazine, 116, 365–374.

Kawate, S., Arima, M., 1998. Petrogenesis of Tanzawa plutonic complex, central Japan: exposed felsic middle of the Izu-Bonin-Mariana arc. The Island Arc, 7, 342–358.

Kobayashi, K., Nakamura, E., 2001. Geochemical evolution of Akagi Volcano, NE Japan: Implications for interaction between island-arc magma and lower crust, and generation of isotopically various magmas. Journal of Petrology, 42, 2303–2331.

Kysar, G., Mortensen, J.K., Lewis, J.F., 1998. U-Pb zircon age constraints for Paleogene igneous rocks of the Sierra Maestra, Southeastern Cuba; implications for short-lived arc magmatism along the northern Caribbean margin. Geological Society of America, Abstracts with Programs, 30, A–185.

Kysar Mattietti, G., 2001. The role of the Paleogene magmatism in the evolution of the northern Caribbean margin, the Sierra Maestra (southern Cuba). Unpublished doctoral dissertation. The George Washington University, 187 pp.

Kysar Mattietti, G., Lewis, J.F., Wysoczanski, R., 2001. Lead isotope study of the Paleogene igneous rocks of the Sierra Maestra, southeastern Cuba. Geological Society of America, Abstracts with Programs, 33, A–304.

Laverov, N., Cabrera, R., 1967. Algunas particularidades de la geología de los alrededores del yacimiento "El Cobre" rela-

cionadas con su génesis. Revista de Geología, Academia de Ciencias de Cuba, 1, 104-121.

Laznicka, P., Notak, P., Schovanek, J., 1970. Geología, Petrografía y Mineralogía de las pendientes meridionales de la Sierra Maestra, al oeste de Santiago de Cuba. Serie oriente, 4, 1–46.

Leroy, S., 1995. Structure et origine de la plaque Caraibe: Implications geodynamiques. Doctoral thesis. Université Pierre et Marie Curie, Paris, 249 pp. Unpublished.

Leroy, S., Mauret, A., Patriat, P., Mercier de Lépinay, B., 2000. An alternative interpretation of the Cayman trough evolution from a reidentification of magnetic anomalies. Geophysical Journal International, 141, 539–557

Lewis, G.E, Straczek, J.A, 1955. Geology of South–Central Oriente province, Cuba. United States Geological Survey, Bulletin, 975D, 171–336.

Lewis, J.F., Escuder Viruete, J., Hernaiz Huerta, P.P., Gutierrez, G., Draper, G., Pérez-Estaún, A., 2002. Subdivisión geoquímica del Arco de Isla Circum-Caribeño, Cordillera Central Dominicana: Implicaciones para la formación, acreción y crecimiento cortical en un ambiente intraoceánico. Acta Geologica Hispanica, 37, 81–122.

Lidiak, E.G., Jolly, W.T., 1996. Circum-Caribbean granitoids: Characteristics and origin. International Geological Review, 38, 1098–1133.

Liu, Y., Genser, J., Handler, R., Friedl, G., Neubauer, F., 2001. $^{40}Ar/^{39}Ar$ muscovite ages from the Penninic/Austroalpine plate boundary, Eastern Alps. Tectonics, 20, 528–547.

MacDougall, I., Harrison, T.M., 1999. Geochronology and thermochronology by the ^{40}Ar-^{39}Ar method. Second edition, Oxford University Press, 269 pp.

Mahlburg Kay, S., Kay, R.W., 1994. Aleutian magmatism in space and time. In: Plafker, G., Berg, H.C. (eds.). The geology of Alaska. Geological Society of America, The geology of North America, G-1, 687–722.

Mandl, G., 1988. Mechanic of tectonic faulting. Models and basic concepts. Zwart, H.J. (ed.). Developments in structural geology. Amsterdam, Elsevier, 407 pp.

Mann, P., Calais, E., Ruegg, J.C., DeMets, Ch., Jansma, P.E., Mattioli, G.S., 2002. Oblique collision in the northeastern Caribbean from GPS measurements and geological observations. Tectonics, 21, 1057, doi: 10.1029/2001TC001304.

Mattietti-Kysar, G., 1999. The role of Paleogene volcanism in the evolution of the northern Caribbean margin. Penrose Conference on "Subduction to Strike-Slip Transitions on Plate Boundaries". Puerto Rico, Abstract-volume, 18–24.

Méndez-Calderón, I., Rodríguez-Crombet, R., Rodríguez, E., Fernández, A., Rodríguez-Mejías, M., Ruiz, R., Hernández, R., 1994. Atlas de rocas de la Sierra Maestra. Empresa Geominera, Santiago de Cuba, 125 pp.

Méndez-Calderón, I., 1997. Apuntes sobre el vulcanismo del Paleógeno en la región Sierra Maestra y características de su composición química. In: Furrazola-Bermúdez, G., Núñez Cambra, K. (eds.). Estudios sobre Geología de Cuba. La Habana, Centro Nacional de Información Geológica, 446–462.

Moreno, B., Grandison, M., Atakan, K., 2002. Crustal velocity model along the southern Cuban margin: implications for the tectonic regime at an active plate boundary. Geophysical Journal International, 151, 632–645.

Pérez-Pérez, C.M., García-Delgado, D., 1997. Tectónica de la Sierra Maestra (Sureste de Cuba). In: Furrazola-Bermúdez, G., Núñez Cambra, K., (eds.). Estudios sobre Geología de Cuba. La Habana, Centro Nacional de Información Geológica, 464–476.

Pindell, J., Kennan, L., 2001. Kinematic evolution of the Gulf of Mexico and Caribbean. 21st Annual Gulf Coast Section Society of Economic Paleontologist and Mineralogist Foundation Bob F. Perkins Research Conference**,** Houston, Texas. Abstract.

Pitcher, W., 1983. Granite types and tectonic environment. In: Hsü, K. (ed.). Mountain building processes. London, Academic Press, 19–40.

Pubellier, M., Mauffret, A., Leroy, S., Marie Vila, J., Amilcar, H., 2000. Plate boundary readjustment in oblique convergence: Example of the Neogene of Hispaniola, Greater Antilles. Tectonics, 19, 630–648.

Remane, J., Cita, M.B., Dercourt, J., Bouysse, P., Repetto, F., Faure-Muret, A. (eds.), 2002. International Stratigraphic Chart. International Union of Geological Sciences: International Commission on Stratigraphy, Paris.

Renne, P., Mattinson, J. M., Hatten, C. W., Somin, T.S., Millán, G., Linares, E., 1989. ^{40}Ar-^{39}Ar and U-Pb evidence for late Proterozoic (Grenville age) continental crust in north-central Cuba and regional tectonic implications. Precambrian Research, 42, 325–341.

Rodríguez-Crombet, R., Rodríguez M., Yassel A., 1997. Características del magmatismo granitoideo de Cuba Oriental (región Sierra Maestra). In: Furrazola-Bermúdez, G., Núñez Cambra, K. (eds.). Estudios sobre Geología de Cuba. La Habana, Centro Nacional de Información Geológica, 446–462.

Rojas-Agramonte, Y., 2003. Tectonic evolution of the Sierra Maestra mountain range, Cuba: from subduction to arc-continent collision and transform motion. Doctoral thesis, Salzburg University, Austria, 143 pp. Unpublished.

Rojas-Agramonte, Y., Neubauer, F., Handler, R., García-Delgado, D.E., Friedl, G., Delgado-Damas, R., 2005, Variation of paleostress patterns along the Oriente Transform Fault, Cuba: Significance for Neogene-Quaternary tectonics of the Caribbean realm. Tectonophysics, 396, 161–180.

Rojas-Agramonte, Y., Neubauer, F., Kröner, A., Wan, Y.S., Liu, D.Y., Garcia-Delgado, D.E., Handler, R., 2004. Geochemistry and age of late orogenic island arc granitoids in the Sierra Maestra, Cuba: evidence for subduction magmatism in the early Palaeogene. Chemical Geology, 213, 307–324.

Rojas-Agramonte, Y., Neubauer, F., García-Delgado, D.E., Handler, R., Friedl, G., Delgado-Damas, R. Tectonic evolution of the Sierra Maestra Mountains, Cuba, during Tertiary times: from arc-continent collision to transform motion. Journal of South American Earth Science (submitted).

Rosencrantz, E., 1990. Structure and tectonics of the Yucatan Basin, Caribbean Sea, as determined from seismic reflection studies. Tectonics, 9, 1037–1059.

Rosencrantz, E., Ross, I.R., Sclater, J.G., 1988. Age and spreading history of the Cayman trough as determined from depth, heat flow and magnetic anomalies. Journal of Geophysical Research, 93, 2141–2157.

Rueda-Pérez, J.S., Arango Arias, E.D., Lobaina Teruel, A., 1994. Algunos resultados del estudio de los movimientos recientes de la corteza terrestre en el poligono geodinámico Santiago de Cuba. Holguín, Cuba, Edición ORISOL, Instituto Cubano de Geodesia y Cartografía, 20 pp.

Schmidt, M.W., 1992. Amphibole composition in tonalite as a function of pressure: an experimental calibration of the Al-in-hornblende barometer. Contributions to Mineralogy and Petrology, 110, 304–310.

Somin, M.L., Millán, G., 1977. Sobre la edad de las rocas metamórficas de Cuba. Informe Científico-Técnico, Academia de Ciencias de Cuba, 80, 11 pp.

Sun, S.S., McDonough, W.F., 1989. Chemical and isotopic systematics of oceanic basalts: implications for mantle composition and processes. In: Saunders, A.D., Norry, M.J. (eds.). Magmatism in ocean basins. Geological Society of London, Special Publication, 42, 313–345.

Tagami, T., Carter, A., Hurford, A.J., 1996. Natural long-term annealing of the fission-track system in Vienna Basin deep borehole samples: constraints upon the partial annealing zone and closure temperature. Chemical Geology, 130, 147–157.

Wagner, G.A., 1968. Fission track dating of apatites. Earth and Planetary Science Letters, 4, 411–415.

Wagner, G.A., Van den Haute, P., 1992. Fission-track dating. Dordrecht, Kluwer Academic Publishers, 285 pp.

Whalen, J.B., 1985. Geochemistry of an island-arc plutonic suite: the Uasilau-Yau Yau intrusive complex, New Britain, Papua New Guinea. Journal of Petrology, 26, 603–632.

White, W.M., Patchett, B.J., 1984. Hf- Nd- and Sr-isotopes and incompatible element abundance in island arcs: implications for magma origins and crust-mantle evolution. Earth and Planetary Science Letters, 67, 167–185.

Manuscript received December 2004;
revision accepted December 2005.

APPENDIX

TABLE 1 | **Compilation of age determinations for Sierra Maestra intrusive rocks.**

Method	Locality	Rock type	Age (Ma)	Reference
K-Ar	Daiquirí Massif	Gabbro	76 ± 3.8	Rodríguez-Crombet et al., 1997
	Daiquirí Massif	Tonalite	44 ± 4	Eguipko and Pérez, 1976
	Daiquirí Massif	Tonalite	54 ± 5	Alioshin et al., 1975
	Daiquirí Massif	Quartz diorite	39 ± 4	Alioshin et al., 1975
	Daiquirí Massif	Quartz diorite	49 ± 6	Laverov and Cabrera, 1967
	Nima-Nima Massif	Plagiogranite	46 ± 6	Laverov and Cabrera, 1967
	Nima-Nima Massif	Quartz diorite	42 ± 5	Eguipko and Pérez, 1976
	Nima-Nima Massif	Quartz diorite	58 ± 5	Laverov and Cabrera, 1967
Conventional U-Pb	Daiquirí Massif	Quartz diorite	49.8 ± 0.2	Kysar et al., 1998
	Daiquirí Massif	Gabbro-diorite	50.2 ± 0.1	Kysar et al., 1998
	Daiquirí Massif	Andesite dyke	50.6 ± 0.1	Kysar et al., 1998
	Daiquirí Massif	Dacite flow	49.7 ± 0.3	Kysar et al., 1998
	Guamá Massif	Quartz diorite	46.9 ± 0.1	Kysar et al., 1998
	Turquino Massif	-	56 (no error provided)	Kysar et al., 1998
U-Pb SRIMP	Daiquirí Massif	Tonalite	50.1 ± 0.5	Rojas-Agramonte et al., 2004
	Daiquirí Massif	Tonalite	310.8 ± 3.4	Rojas-Agramonte et al., 2004
	Nima-Nima Massif	Tonalite	50.5 ± 0.5	Rojas-Agramonte et al., 2004
	Nima-Nima Massif	Tonalite	50.1 ± 0.5	Rojas-Agramonte et al., 2004
	Peladero Massif	Tonalite	48.2 ± 0.4	Rojas-Agramonte et al., 2004
	Turquino Massif	Tonalite	55.4 ± 0.7	Rojas-Agramonte et al., 2004
	Turquino Massif	Trondhjemite	60.2 ± 2.6	Rojas-Agramonte et al., 2004
$^{40}Ar/^{39}Ar$	Nima-Nima Massif	Tonalite	54 ± 4	This paper
	Peladero Massif	Tonalite	50 ± 2	This paper
Zircon Fission track	Daiquirí Massif	Tonalite	36 ± 4	This paper
	Nima-Nima Massif	Tonalite	39 ± 4	This paper
	Nima-Nima Massif	Tonalite	32 ± 3	This paper
	Nima-Nima Massif	Tonalite	41 ± 3	This paper
	Peladero Massif	Tonalite	44 ± 4	This paper
Apatite Fission track	Nima-Nima Massif	Tonalite	44 ± 13	This paper
	Turquino Massif	Tonalite	31 ± 10	This paper

TABLE 2 | **Analytical data from multi-grain incremental heating ^{40}Ar-^{39}Ar analyses of biotite from granitoids of the Sierra Maestra, SE-Cuba. Errors are 1-sigma.**

Sample:	CU40 Biotite (Peladero)						
J-Value:	0.01892 +/- 0.000189						
Step	$^{36}Ar/^{39}Ar$	$^{37}Ar/^{39}Ar$	$^{40}Ar/^{39}Ar$	$\%^{39}Ar$	$\%^{40}Ar^*$	age	+/-
	meas.	corr.	meas.			[Ma]	[Ma]
1	0.04929	0.1782	14.83	7.2	1.8	8.8	5.2
2	0.01093	0.0912	4.6	2.1	29.8	46	14.4
3	0.01266	0.0735	4.91	6	23.9	39.2	5.9
4	0.0055	0.0715	3.23	4.7	49.6	53.6	6.7
5	0.00187	0.0487	2.19	5.6	74.7	54.5	5.6
6	0.00221	0.0534	2.1	3.6	68.8	48.2	8.1
7	0.00185	0.0734	2.23	5.5	75.5	56.2	5.5
8	0.00523	0.043	3.16	13.5	51.2	54.1	2.5
9	0.00257	0.0511	2.37	14.5	67.9	53.7	2.5
10	0.00893	0.0642	4.27	8.6	38.2	54.4	3.8
11	0.00326	0.1014	2.63	12	63.4	55.8	2.4
12	0.00092	0.1308	1.85	7.2	85.2	52.8	3.7
13	0.00022	0.0341	1.68	4.1	96.2	53.8	5.8
14	0.0002	0.0134	1.58	5.3	96.3	50.6	4.2
total	0.00741	0.07457	3.67	100	40.4	49.6	0.5
Integrated steps 4 - 14					**84.6**	**53.8**	**3.8**

Sample:	CU29 Biotite (Nima Nima)						
J-Value:	0.01897 +/- 0.000190						
Step	$^{36}Ar/^{39}Ar$	$^{37}Ar/^{39}Ar$	$^{40}Ar/^{39}Ar$	$\%^{39}Ar$	$\%^{40}Ar^*$	age	+/-
	meas.	corr.	meas.			[Ma]	[Ma]
1	0.01213	0.0275	4.478	2.9	20	29.9	5.9
2	0.00454	0.03461	2.758	5.9	51.3	47.4	2.7
3	0.00568	0.01406	3.057	1.8	45.1	46.1	9
4	0.00748	0.06263	3.273	1.6	32.5	35.7	10.1
5	0.00633	0.03413	2.923	3.9	36	35.2	4.1
6	0.0026	0.02576	2.04	2.7	62.4	42.6	4.5
7	0.00238	0.02239	2	3.4	64.8	43.3	3.7
8	0.00147	0.00391	1.91	2.5	77.2	49.3	4.9
9	0.00188	0.02105	2.055	4.1	73	50.1	3.8
10	0.003	0.03782	2.487	3.6	64.3	53.5	3.9
11	0.00129	0.02817	1.993	4.9	80.9	53.9	3.3
12	0.0012	0.02611	1.859	7.7	80.9	50.3	2.1
13	0.0006	0.03586	1.801	8.9	85.3	51.4	1.7
14	0.00074	0.02797	1.756	10.2	87.5	51.4	1.6
15	0.00091	0.02853	1.687	5.5	84.1	47.5	2.9
16	0.00059	0.15032	1.595	12.6	89	47.8	1.4
17	0.00064	0.04516	1.704	6	88.8	50.7	2.6
18	0.00079	0.27907	1.66	5.9	86	48.4	2.6
19	0.00089	0.07971	1.642	6.1	84	46.3	2.7
total	0.00203	0.06149	2.027	100	70.5	47.9	0.5
Integrated steps 8 - 19				**77.9**		**49.9**	**2.4**

TABLE 3 **Zircon fission track analytical data. ρ = track density (x10^6 tracks cm^{-2}); (N) = number of tracks counted; s, i and d denote, spontaneous, induced tracks and tracks in the fluence monitor glass, respectively. Samples were dated using the external detector method (Hurford et al., 1983).**

Sample	Mineral /No. of crystals	Dosimeter ρd (Nd) (x106 cm-²)		Spontaneous track density ρs (Ns) (x106 cm-²)		Induced track density ρi (Ni) (x106 cm-²)		Pooled Age ±1σ (Ma)	Proba-bility (%)	U (ppm)
CU5 (Daiquirí)	9	0.4506	(4506)	6.598	(386)	4.735	(277)	36±4	80	287
CU29 (Nima-Nima)	8	0.4506	(4506)	6.582	(520)	4.354	(344)	39±4	80	264
CU30 (Nima-Nima)	8	0.4506	(4506)	3.262	(517)	2.669	(423)	32±3	23	162
CU32 (Nima-Nima)	15	0.4506	(4506)	3.829	(987)	2.425	(625)	41±3	22	147
CU40 (Peladero)	7	0.4506	(4506)	11.981	(623)	7.077	(368)	44±4	45	428

TABLE 4 **Apatite fission track analytical data. ρ = track density (x10^6 tracks cm^{-2}); (N) = number of tracks counted; s and i denote, spontaneous and induced tracks, respectively. Samples were dated using the population method (Wagner, 1968, Wagner and Van der Haute, 1992).**

Sample code	Number of grains or grids	Spontaneous tracks		Induced tracks		Error	Neutron flux	Fission track age in Ma
	(n_s/n_i)	N_s	ρ_s (10^6 cm^{-2})	N_i	ρ_i (10^6 cm^{-2})	1 σ of ρ_s/ρ_i (%)	(10^{14} cm^{-2})	error is 1σ
CU30 (Nima-Nima)	30/20	20	0.0417	16	0.05	30	10.68	44 ± 13
CU60 (Turquino)	20/10	17	0.0531	15	0.0938	34	11.02	31 ± 10

TABLE 5| **Representative chemical composition of plagioclase and amphibole. b.d. - below detection limit.**

Plagioclase	CU5 (Daiquirí)		CU10 (Daiquirí)		CU29 (Nima-Nima)	CU30 (Nima-Nima)	CU60 (Turquino)
	core	rim	core	rim	core	core	core
SiO_2(wt%)	58.9	64.6	54.5	64.25	52.14	55.48	56.72
Al_2O_3	25.57	22.13	28.67	22.47	30.13	27.92	26.53
MgO	0.02	0.01	0.01	b.d.	0.005	0.03	0.01
Na_2O	6.86	9.23	5.01	8.89	3.81	5.43	6.44
CaO	8.1	3.64	11.55	4.11	13.62	10.61	9.09
K_2O	0.35	0.3	0.16	0.38	0.13	0.14	0.17
TiO_2	0.03	0.02	0.03	b.d.	0.01	0.01	0.02
Fe_2O_3	0.22	0.15	0.23	0.15	0.4	0.38	0.25
MnO	0.02	<0.01	<0.01	0.03	b.d.	0.01	0.01
Cr_2O_3	0.06	0.02	b.d.	b.d.	b.d.	b.d.	b.d.
Total	100.1	100.1	100.2	100.3	100.3	100	99.23
Si	2.63	2.85	2.46	2.83	2.36	2.5	2.57
Al	1.35	1.15	1.52	1.17	1.61	1.48	1.41
Na	0.59	0.79	0.44	0.76	0.33	0.47	0.56
Ca	0.39	0.17	0.56	0.19	0.66	0.51	0.44
K	0.02	0.02	0.01	0.02	0.01	0.01	0.01
Amphibole	**CU5**	**CU10**		**CU29**	**CU30**	**CU60**	
	rim	core	core	core	rim	-	-
SiO_2(wt%)	47.43	52.64	47.44	46.45	48.16	49.77	42.69
Al_2O_3	5.39	2.5	6.3	7.11	5.34	1.33	8.1
MgO	10.13	14.45	13.44	12.6	10.49	9.25	3.77
Na_2O	0.99	0.46	1.46	1.63	0.92	0.38	0.93
CaO	10.05	10.85	10.99	11.09	10.2	2.75	11.14
K_2O	0.39	0.16	0.32	0.32	0.39	0.04	0.55
TiO_2	0.58	0.3	1.58	1.79	0.29	0.19	0.12
FeO	21.41	16.63	15.99	16.76	21.46	32.12	29.18
MnO	1.62	0.88	0.46	0.35	b.d.	2.06	1.25
Cr_2O_3	0.04	0.01	<0.01	b.d.	0.95	b.d.	b.d.
Total	98.06	98.89	98	98.1	98.23	97.89	97.73
Si	7.11	7.6	6.96	6.83	7.16	7.74	6.69
Al	0.95	0.42	1.09	1.23	0.94	0.24	1.49
Mg	b.d.	3.11	2.94	2.76	2.33	2.14	0.88
Na	0.29	0.13	0.42	0.46	0.27	0.11	0.28
Ca	1.61	1.68	1.73	1.75	1.62	0.46	1.87
K	0.07	0.03	0.06	0.06	0.07	0.01	0.11
Ti	b.d.	0.03	0.17	0.2	0.03	0.022	0.01
Fe^{2+}	2.13	1.77	1.61	1.64	2.07	4.177	2.97
Fe^{+}	0.55	0.25	0.35	0.42	0.6	b.d.	0.85

TABLE 6| **Phases of deformation in the Sierra Maestra and fault patterns characterizing palaeostress phases D_1-D_6 (from Rojas-Agramonte et al., submitted).**

	Sierra Maestra			Gran Piedra		Fault pattern scheme
	Structures	**Interpretation**		**Structures**	**Interpretation**	
D1	Extensional tectonics, associated mainly with N-S trending extensional veins and dikes	Predominant E-W and less radial extension	D1	Extensional tectonics related with extensional veins and dikes	E-W to nearly NW-SE extension and NE-SW compression	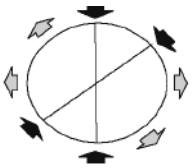
D2	Reverse, dextral and sinistral strike-slip faults. Isoclinal folds, normal faults and calcite-filled veins	N-S to NE-SW compression; extension varying from E-W to nearly NW-SE	D2	"Thrusts, reverse and dextral strike-slip faults, less sinistral strike-slip faults; overturned folds"	N-S compression	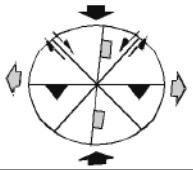
D3	E-W trending normal faults and calcite-filled veins	N-S to nearly NNE-SSW and NNW-SSE extension	D3	E-W trending normal faults and calcite-filled veins	N-S extension	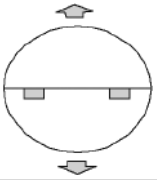
D4	Reverse, dextral and sinistral strike slips faults. Normal faults	NE-SW to nearly ENE-WSW compression and NW-SE extension	D4	Dextral N-S trending strike-slip faults and calcite-filled veins	NE-SW compression and NW-SE extension	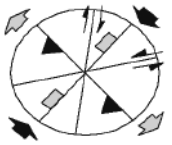
D5	Reverse, dextral and sinistral strike-slip faults. Normal faults and extensional calcite-filled veins NE-SW extension	NW-SE compression	D5	Sinistral strike-slip and normal faults	NW-SE compression and NE-SW extension	
D6	Reverse, sinistral and dextral strike-slip faults. Normal faults	E-W compression and N-S extension and N-S to nearly NNW-SSE extension	D6	Sinistral WNW-trending strike-slip faults	E-W compression